Summer 2020

Observations and Simulations of Fire Weather Phenomena Across Scales

Matthew James Brewer
San Jose State University

OBSERVATIONS AND SIMULATIONS OF FIRE WEATHER PHENOMENA ACROSS SCALES

A Thesis

Presented to

The Faculty of the Department of Meteorology and Climate Science

San Jose State University

In Partial Fulfillment

of the Requirements for the Degree

Master of Science

by

Matthew James Brewer

August 2020

The Designated Thesis Committee Approves the Thesis Titled

OBSERVATIONS AND SIMULATIONS OF FIRE WEATHER PHENOMENA ACROSS SCALES

by

Matthew James Brewer

APPROVED FOR THE DEPARTMENT OF METEOROLOGY AND CLIMATE SCIENCE

SAN JOSÉ STATE UNIVERSITY

August 2020

Craig Clements, Ph.D.	Department of Meteorology and Climate Science
Alison Bridger, Ph.D.	Department of Meteorology and Climate Science
Sen Chiao, Ph.D.	Department of Meteorology and Climate Science

ABSTRACT

OBSERVATIONS AND SIMULATIONS OF FIRE WEATHER PHENOMENA ACROSS SCALES

by Matthew James Brewer

The need for a better understanding of wildfires and how the atmosphere affects them provided the motivation for this work. The November 2018 Camp Fire quickly became the deadliest and most destructive wildfire in California history. In chapter 1, we investigate the contribution of meteorological conditions and a downslope windstorm event that occurred during the 2018 Camp Fire. Results show that this event was associated with mid-level and surface synoptic scale processes which created conditions favorable for a North wind event. Sustained surface winds between 3–6 m s^{-1} were observed with gusts of over 25 m s^{-1}. The meteorological conditions of the event were well forecasted, and the severity of the fire was not surprising given the fire danger potential for that day. The usage of small unmanned aircraft systems (sUAS), may help to provide new observations in extreme environments such as the Camp Fire. The Fire and Smoke Model Evaluation Experiment offered a unique opportunity of a large controlled wildfire, which allowed measurements that cannot generally be taken during an active wildfire. This study highlights the use of DJI Matrice 200 that was equipped with a TriSonica Mini Wind and Weather station sonic anemometer in order to sample the fire environment in an experimental and controlled setting. The system was tested against an RM-Young 81000 sonic anemometer mounted at 6 and 2 m AGL to assess any bias in the sUAS platform. Preliminary data show that this system can be useful for taking vertical profiles, in addition to being used in place of tower measurements.

ACKNOWLEDGMENTS

First, I would like to thank my advisor Dr. Craig Clements for his guidance and support throughout my time at San Jose State. I am grateful for the knowledge and experience I gained which would not have been possible without Dr. Clements. Additionally, I would like to thank Drs. Sen Chiao and Alison Bridger for taking time out of their busy schedules to be on my thesis committee.

I would also like to thank the members of the Fire Weather Laboratory for the countless adventures, hours of lab chit-chats, and unwavering support. Additionally, I would like to thank my fellow graduate students for coding help, presentation practice, and proof reading. Furthermore, I would like to thank all the staff in the Department of Meteorology and Climate Science for the support and knowledge I gained through my various classes.

Finally, I would like to thank my family for their support in moving me across the country, being okay with me driving towards wildfires, and the work ethic that they instilled within me. I am extremely grateful for the support of Courtney Trudeau, whose hours of proof reading, presentation help, and encouragement have helped get me where I am today.

This research would also not be possible without the numerous grants including National Science Foundation award #1807774 and AGS-1151930, in addition to U.S. Forest Service, Pacific Northwest Research Station 19-CR011261987-062.

TABLE OF CONTENTS

LIST OF TABLES

LIST OF FIGURES

LIST OF ABBREVEATIONS

ACM2 – Asymmetric Convection Model version 2
AGL – Above Ground Level
ARW – Advanced Research WRF
AWB – Anti-cyclonic Rossby Wave Breaking
CAA – Cold Air Advection
COA – Certificate of Authorization
CSU-MAPS – California State University Mobile Atmospheric Profiling System
DW – Diablo Winds
EMC – Environmental Modelling Center
FASMEE – Fire and Smoke Model Evaluation Experiment
FFWI – Forsberg Fire Weather Index
FMC – Fuel Moisture Content
FM-100 – 100 hour Fuel Moisture Content
GFS – Global Forecast System
h – Hour
HDW – Hot Dry Windy
hPa – Hectopascal
HRRR – High Resolution Rapid Refresh
IMU – Inertial Measurement Unit
km – Kilometer
Lat – Latitude
Lidar – Light Detection and Ranging
Lon – Longitude
M200 – DJI Matrice 200 v2
m – Meter
mm – Millimeter
μm – Micrometer
$m\ s^{-1}$ – Meter per Second
MSLP – Mean Sea Level Pressure
NCEP – National Center for Environmental Prediction
NEXRAD – Next Generation Radar
NFDRS – National Fire Danger Rating System
NWS – National Weather Service
PBL – Planetary Boundary Layer
PRISM – Parameter-elevation regression on Independent Slopes Model
PG&E – Pacific Gas and Electric
PV – Potential Vorticity
Radar – Radio Detection and Ranging
RAWS – Remote Automated Weather Stations
RH – Relative Humidity
RMSE – Root Mean Square Error
RMY – RM Young 81000

ROS – Rate of Spread
RRTM – Rapid Radiative Transfer Model
SAW – Santa Ana Winds
SFBA – San Francisco Bay Area
Sodar – Sonic Detection and Ranging
UAS – Unmanned Aerial Systems
UAV – Unmanned Aerial Vehicles
USFS – United States Forest Service
VPD – Vapor Pressure Deficit
WRF – Weather Research and Forecasting
WSR-88D – Weather Surveillance radar – 1988 Doppler

Chapter 1

The 2018 Camp Fire: Meteorological Analysis Using in situ Observations and Numerical Simulations

Section 1: Introduction and Background

Many of California's largest, deadliest, and destructive wildfires occur during strong downslope windstorms. These strong and typically hot and dry downslope winds, which occur on the lee side of mountains, can be generically referred to as foehn winds (Brinkman 1971; Whiteman 2000). Mountain waves and ensuing downslope windstorm dynamics have been observed and modeled extensively (Durran 2003, 1990; Klemp and Lilly 1974; Cao 2015; Smith 1985; Markowski and Richardson 2010, among others). The basic conditions necessary for amplification of mountain waves, which lead to downslope windstorms, are strong winds between 7–15 m s^{-1}, flowing within 30° of perpendicular to the ridge line, and an inversion or layer of high static stability, located near crest height upstream of the mountain (Durran 1990). In California, these foehn winds are referred to by a number of different names, most notably, Santa Ana winds (SAW) and Diablo winds (DW). SAW occur in Southern California during the fall, winter, and into early spring, with occurrence peaking in December (Westerling et al. 2004; Raphael 2003). These winds are characterized by hot, gusty offshore winds, which promote the spread and ignition of wildfires. Mechanisms forcing SAW include a strong surface pressure gradient between coastal troughs and high-pressure systems over the Great Basin, as well as a temperature gradient between the cooler inland deserts and the coast (Raphael 2003; Edinger et al. 1964). Additional mid-level forcing for SAW includes 850 hPa cold air

advection (CAA) and negative vorticity advection at 500 hPa (Abatzoglou et al. 2013; Rolinski et al. 2019). These hot, gusty conditions have fanned many large fires including, the Woolsey Fire in 2018, Thomas Fire in 2017, Witch Fire in 2007, and the 2003 Cedar and Old Fires (CalFire 2019). DW typically refer to the foehn winds that occur in the San Francisco Bay Area (SFBA) region; notable occurrences include the Wine Country/Napa county fires of 2017, specifically the Tubbs Fire, and the Tunnel Fire in the Oakland Hills in 1991 (Bowers 2018; Monteverdi 1973; C. Smith 2018). These winds are similar to SAW, with hot, dry, gusty downslope winds that predominantly occur in the fall (Bowers 2018; Smith et al. 2018).

Additionally, similar to SAW events, a DW forcing mechanism includes a coastal inverted trough and a high-pressure system in the Pacific Northwest or Great Basin regions of the Western United States (Bowers 2018; Monteverdi 1973; C. Smith 2018). The DW nomenclature has also been associated with the foehn winds in the western Sierra Nevada due to their similarities to the DW. However, the occurrence of foehn winds on the western Sierra Nevada does not mean that the DW will occur in the SFBA as well and vice-versa. Therefore, we classify downslope windstorms in the western Sierra Nevada as North winds following Whiteman (2000) and Werth et al. (2011). Additionally, we use North winds in this study to further differentiate between the two geographic regions of the SFBA and the Sierra Nevada and refer to this event as the downslope windstorm.

The Camp Fire ignited during a North wind event, which spread the fire rapidly and caused it to burn roughly 28,000 ha in less than 24 h (CalFire 2019). This North wind

event brought gusts of over 15 m s^{-1} to the surface in an environment with record dry fuels. The Camp Fire was first reported at 06:33 PST 8 November 2018. The ignition was in the area of Camp Creek Road in the Feather River Canyon northeast of Pulga, CA (CalFire 2018). Strong winds, >20 m s^{-1}, accelerated down the canyon and likely contributed to both the start of the fire and rapid spread rate. The high rate of spread (ROS) pushed the fire through the communities of Concow, Paradise, and Magalia by the end of the day on 8 November 2018, destroying and damaging a majority of the buildings in its path. This extreme fire behavior can be largely attributed to the strong sustained and gusty winds and ember transport. The winds fanned the fire pushing the fire front at a high ROS. However, lofted fire brands may have been the main driver behind the high ROS. These fire brands were observed traveling distances of >1.5 km ahead of the main fire front, causing spot fires and igniting many structures (CalFire 2018). In total, the fire destroyed roughly 19,000 structures and had burnt roughly 62,000 ha once the fire was fully contained 17 days later on 25 November 2018 (CalFire 2018). This downslope windstorm included aspects of both SAW and DW events. There are few, if any, examples in the literature of these downslope windstorms occurring in the western Sierra Nevada, especially regarding extreme fire weather. This case study of the meteorological conditions associated with the Camp Fire is motivated by the gap in the literature regarding this type of North wind event in addition to the magnitude of destruction associated with the fire. Results from this case study may be useful for forecasters in the private and public sector predicting these downslope windstorms for red flag warnings and power shut off programs. This paper examines the meteorological context prior to

and during the 2018 Camp Fire using both observations and numerical modeling. The structure of this paper is as follows: Section 2 describes the data and methods used in this analysis, Section 3 details the observed and modeled conditions prior to ignition as well as the conditions associated with the downslope windstorm event, Section 4 presents model verification metrics, and Section 5 summarizes the results and presents further discussion.

Section 2: Data and Methodology

Section 2.1: Observations

Many different observational datasets were used in this analysis of the conditions prior to and during the Camp Fire, including surface weather station observations, precipitation data, and remotely sensed observations. In order to assess the environment prior to the fire, we investigated October 2018 precipitation departures from climatology based on the climatological period of 1981–2010. These departures were made using the National Weather Service (NWS) hydrologic precipitation service quantitative precipitation estimate. The Stage IV precipitation data are quality controlled, using radar and rain gauge estimates obtained from NWS River Forecast Centers, and gridded by the National Centers for Environmental Prediction (NCEP) at 4 km resolution (NCEP 2000). The climatological normal precipitation is derived from the parameter-elevation regressions on independent slopes model (PRISM) climate model data at 4 km grid spacing produced by the PRISM climate group at Oregon State University (NWS 2018).

Surface *in situ* data were obtained from the United States Forest Service (USFS) remote automated weather station (RAWS) network and the Pacific Gas and Electric

(PG&E) station network (Table 1). RAWS makes up an interagency network of surface stations that are primarily used to assess fire danger in remote locations throughout the United States.

Table 1. Description of weather stations used in this analysis.

Station Name	Station ID	Lat/Lon	Elevation(m)	Type	Record Span
Jarbo Gap	JBGC1	39.74, -121.49	773	RAWS	2003/04/21 –Current
Openshaw	CICC1	39.59, -121.64	82	RAWS	1999/12/02 –Current
Saddleback	SLEC1	39.63, -120.86	2033	RAWS	2001/06/26 –Current
Colby Mtn.	CBXC1	40.14, -121.52	1830	RAWS	2015/06/08 –Current
Humbug Summit	HMRC1	40.11, -121.38	2046	RAWS	2012/07/24 –Current
Stirling City	PG131	39.91, -121.53	1143	PG&E	2018/10/02 –Current
Red Hill Lookout	PG129	40.03, -121.18	1930	PG&E	2018/10/11 –Current

RAWS are sited according to the National Wildfire Coordinating Group Standards for Fire Weather Stations and the National Fire Danger Rating System (NFDRS) protocol, with winds measured at 6.1 m (20 ft) above ground level (AGL) and the air temperature and relative humidity (RH) measured between 1.2–2.5 m (4–8 ft) AGL (Zachariassen et al. 2003). Wind and RH data are collected from 10 min averages prior to the hourly transmission time, while temperature is the instantaneous sample at the hour (Zachariassen et al. 2003). Site metadata and data collected from RAWS are used to calculate dead fuel moisture content. In this analysis, NFDRS 100-h fuel moisture content (FM-100) was used to investigate fuel moisture prior to ignition (Cohen and Deeming

1985). This fuel class represents dead fuels that take 100 h to reach 2/3 of equilibrium with the local environment, and range in size from 25 mm to 75 mm (Deeming et al. 1978). FM-100 were chosen due to their slower response time, which shows larger scale variations in the weather, and for the size of the fuel class.

In total, five RAWS, (Jarbo Gap, Openshaw, Colby Mountain, Saddleback, and Humbug) and two PG&E weather stations (Stirling City and Red Hill Lookout) were used in this analysis, and station locations are shown in Figure 1B. In order to assess the climatology of FM-100, the entire record of each RAWS was used to calculate daily minimum and average FM-100 and compared these data to daily FM-100 from 1 October 2018 through 10 November 2018. The time span from 00:00 PST 7 November 2018–00:00 PST 10 November 2018 was used to analyze the downslope windstorm conditions. Additionally, a sounding from the NWS in Reno, Nevada was obtained for 12:00 UTC 8 November 2018.

In conjunction with surface *in situ* observations, this analysis takes advantage of remotely sensed observations from lidar and radar. The California State University Mobile Atmospheric Profiling System (CSU-MAPS) was deployed to the Camp Fire on 8 November 2018 (Clements and Oliphant 2014). The CSU-MAPS was equipped with a Halo Photonics, 1.5 μm scanning Doppler lidar, which has a resolution of 18 m and a range of 9.6 km. The lidar records attenuated backscatter and Doppler radial velocity data, as well as vertical wind profiles. Vertical wind profiles near the fire front were measured at two locations (Figure 1B).

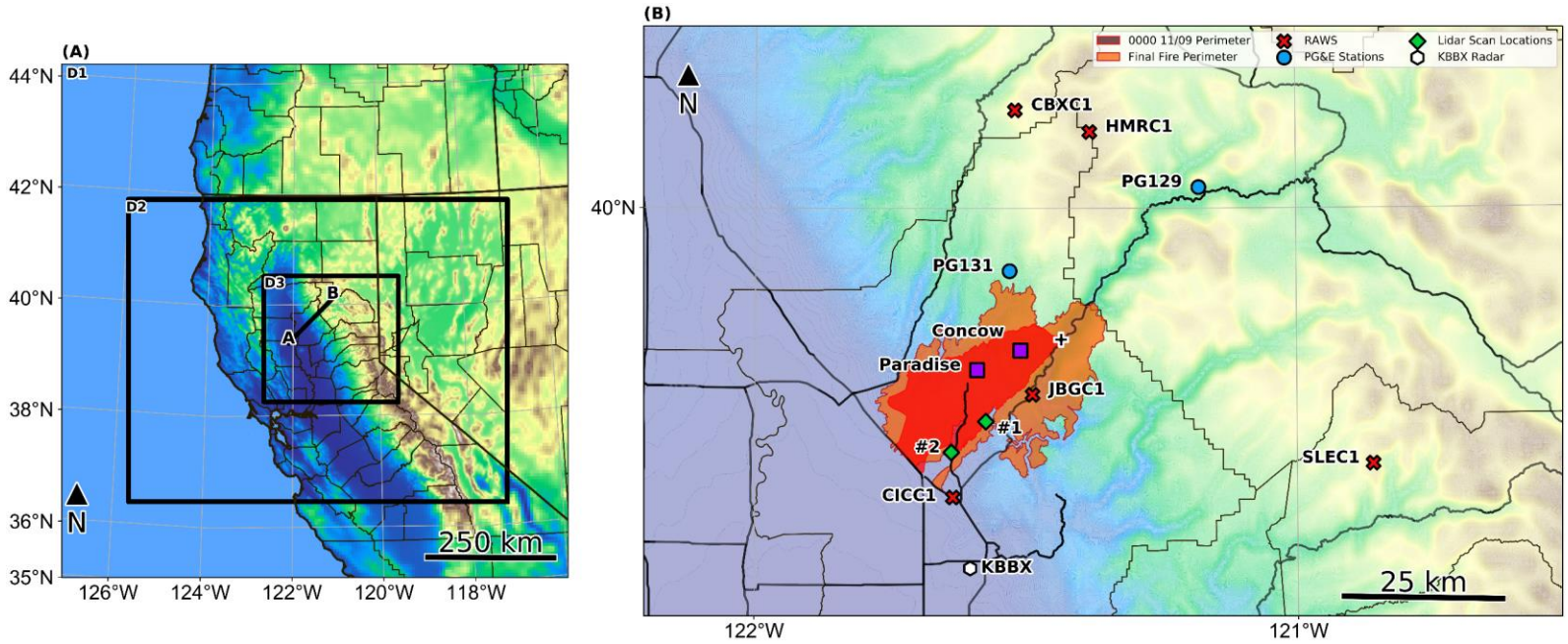

Figure 1. (A) Domains used in weather research and forecasting (WRF)-advanced research WRF (ARW) simulations and topography shaded. Outer domain D1 has a grid spacing of 6 km, with inner domains D2 and D3 grid spacing of 2 km and 0.666 km, respectively. Line AB represents the cross-section used in this analysis; (B) WRF model terrain (shaded) with locations of remote automated weather station (RAWS) (Xs), Pacific Gas and Electric (PG&E) stations (circles), lidar scan locations (diamonds), KBBX radar (hexagon), approximate ignition point ("+"), and city locations (squares). Shaded in red are Camp Fire perimeters with the inner perimeter from 00:00 PST 9 November 2018 and the outer perimeter being the final perimeter.

Location one was along Pentz Road on the southern flank of the fire and location two was located at the temporary incident command post at Butte College, also roughly on the southern flank. Radar data from the smoke plume were obtained from the KBBX Beale Air Force Base, California NWS next-generation radar (NEXRAD) weather surveillance radar-1988 Doppler (WSR-88D) S-band radar for 8–9 November 2018 (Figure 1B) (NWS Radar 1991). Data from both the lidar, radar, and surface stations are used in this analysis to validate model simulations and assess fire risk.

Section 2.2: Modeled data

The analysis of synoptic weather patterns prior to and during the Camp Fire were made using the global forecast system (GFS) analysis products from NCEP at 0.5° grid spacing 7–9 November 2018 (EMC, 2018). The GFS was chosen due to its widespread use in operational fire weather forecasts in the United States. We used the GFS data to investigate the mid-level synoptic evolution at 700 hPa. This level was analyzed due to being just above crest height throughout much of the Sierra Nevada. The specific products analyzed at 700 hPa include geopotential heights, temperature, wind, and temperature advection. Additionally, the surface conditions were analyzed using mean sea level pressure (MSLP). These products give insight on the synoptic driver behind the North wind event that occurred in the western Sierra Nevada on 8 November 2018. In addition to the GFS, a high-resolution simulation was used to analyze fine-scale winds, specifically the wind structure associated with the downslope windstorm. The simulation was made using version 4.0 of the weather research and forecasting (WRF) model's advanced research WRF (ARW) core (Skamarock et al. 2008). WRF simulation utilized

2-way nesting for three nested domains with grid spacing of 6 km, 2 km, 0.666 km, and 80 vertical levels; the domains with respective grid spacing are shown in Figure 1A. The simulation was integrated for 48 h from 00:00 UTC 8 November 2018–00:00 UTC 10 November 2018, with initialization and boundary conditions from the 12 km NCEP North American Mesoscale model. Table 2 lists WRF model physics parameterizations used in this simulation.

Table 2. WRF model parameterization name and namelist option.

Parameterization type	**Physics scheme**
Microphysics	Thompson graupel (8)
Radiation	RRTMG (4)
Surface layer physics	Pleim-Xiu (7)
Planetary Boundary Layer	ACM2 (7)

Consistent with Fovell and Gallagher (2018) and Cao and Fovell (2016, 2018), we tested a number of different physics configurations, including a HRRR-like setup, but found that the combination of the Pleim-Xiu land surface model and the Asymmetric Convection Model version 2 (ACM2) PBL scheme performed best overall (not shown) (Pleim and Aijun Xiu 1995; Pleim 2007). Additionally, this analysis compared WRF 10 m wind speed and direction directly to 6.1 m RAWS wind observations. We decided to not adjust the wind measurements from 10 m to 6.1 m due to the fact that operational weather models typically only report 10 m winds and recent studies (Cao and Fovell

2016; Fovell and Gallagher 2018) found that adjusting measurements lower had little effect on results.

Section 3: Results

Section 3.1: Precipitation and Fuels

Live and dead fuels typically reach their minimum in fuel moisture content (FMC) in the fall, September–October, due to the lack of precipitation, high temperatures, and low RH experienced throughout the summer. FMC start to recover in the late fall as precipitation, lower temperatures, and higher RH become more common. However, a lack of precipitation throughout October 2018 led to departures from the long-term climatological normal of 50–100 mm of precipitation in the area of the Camp Fire (Figure 2).

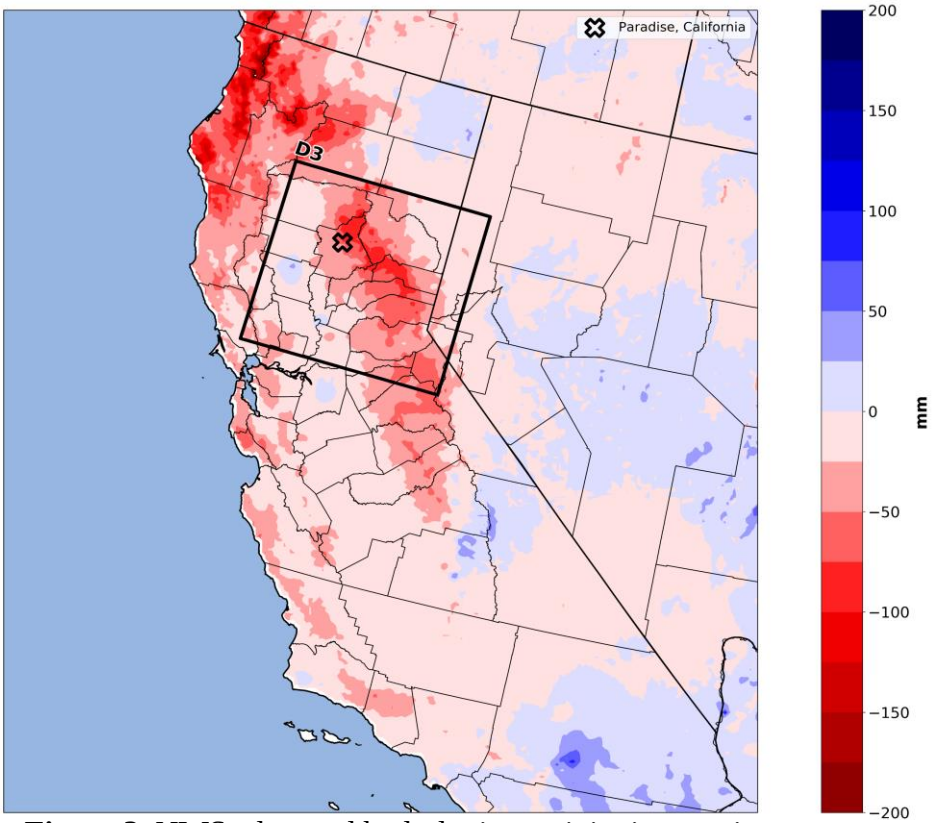

Figure 2. NWS advanced hydrologic precipitation service quantitative precipitation estimate departures from normal based on 1981–2010 climatology.

The lack of precipitation during the month of October led to continued drying of fuels in the region. The only precipitation occurred between 3–5 October 2018, when the FM-100 at all RAWS reached a relative maximum and declined through 25 October 2018 (Figure 3). Between 25–30 October 2018, an increase in RH (not shown) led to increased FM-100 (Figure 3).

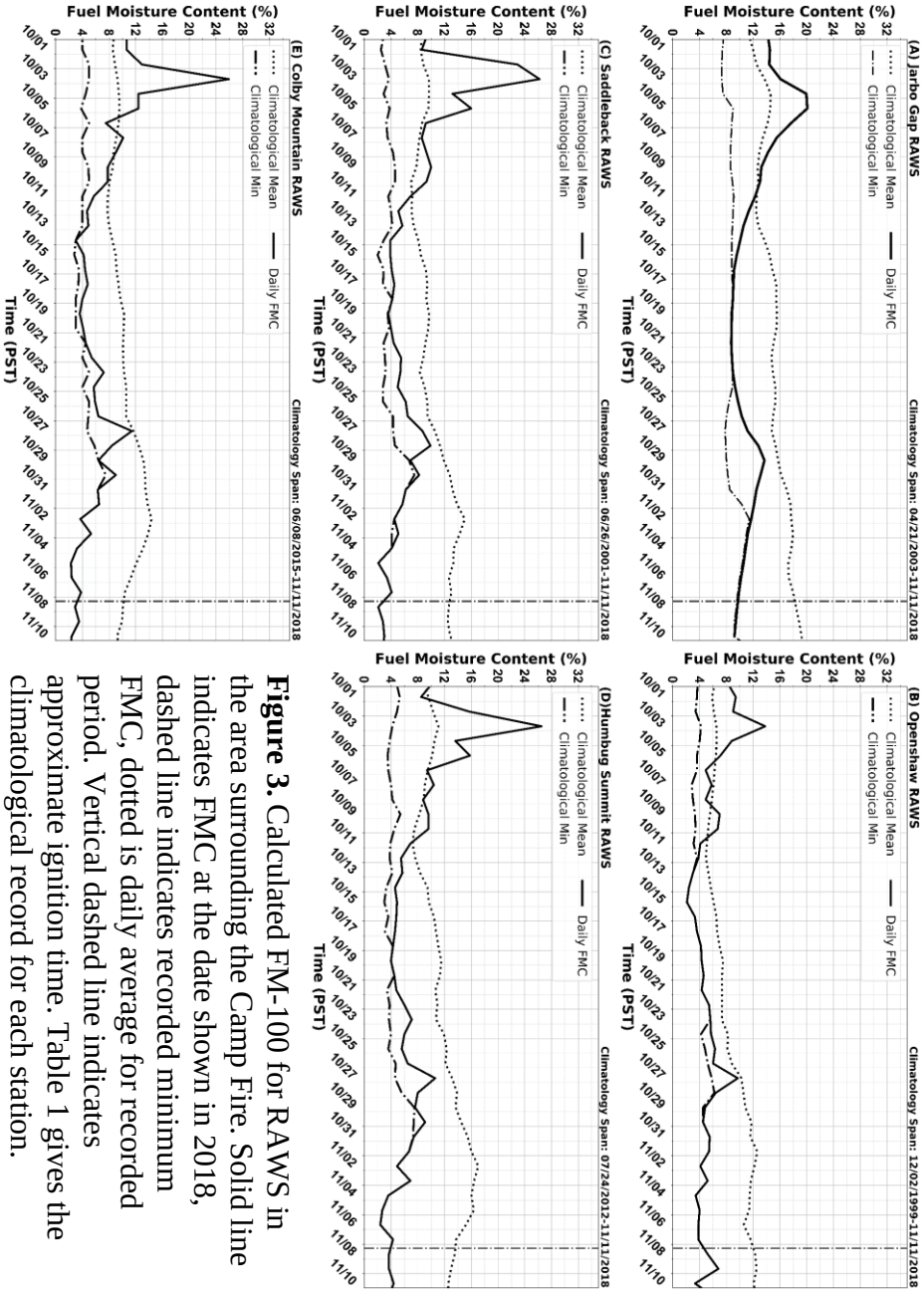

Figure 3. Calculated FM-100 for RAWS in the area surrounding the Camp Fire. Solid line indicates FMC at the date shown in 2018, dashed line indicates recorded minimum FMC, dotted is daily average for recorded period. Vertical dashed line indicates approximate ignition time. Table 1 gives the climatological record for each station.

Throughout the remainder of October and into November, leading up to the ignition of the fire, no precipitation or prolonged high RH was measured at any of the nearby RAWS sites. This lack of precipitation and lower RH led to all RAWS station reaching within 0.5% of their lowest calculated FM-100 in the station's recording period, prior to the fire and through 10 November 2018 (Table 1). The average FM-100 on the day of ignition was 4.88%, with the lowest FM-100 tied between Openshaw and Colby Mountain RAWS of 3.8%.

3.2. Synoptic Overview

The mid-level evolution of geopotential heights, winds, and temperature advection from 10:00 PST 7 November 2018–10:00 PST 9 November 2018 is shown in Figure 4A–E. Figure 4A shows an amplified ridge extending well into British Columbia, Canada, which created northerly flow along the Canadian and United States western coast advecting colder air into the region over southwest Oregon and northwest California. Twelve hours later (Figure 4B), a short-wave trough became embedded within the larger ridge over northern California, which was likely caused by the height falls associated with the CAA in the layer. This persistent CAA continued to deepen the shortwave trough and erode the base of the ridge, potentially contributing to anticyclonic Rossby wave breaking (AWB) as the CAA continued to deepen the shortwave and tilt the ridge (Figure 4C). Rossby wave breaking can be defined by the irreversible deformation potential vorticity (PV) contours on isentropic surfaces over a longitudinally confined region, which are associated with stratospheric PV streamers intruding the troposphere (Appenzeller and Davies 1992; Mcintyre and Palmer 1983; Mcintyre 1984). Near the

start of the AWB event at 10:00 PST 8 November 2018, there is a longitudinal gradient >5 PVU along the 120° W meridian on the 330 K isentropic surface, consistent with a high PV streamer intrusion (not shown). The shortwave trough and the AWB at 700 hPa aligned the winds with the Sierra Nevada ridge crest.

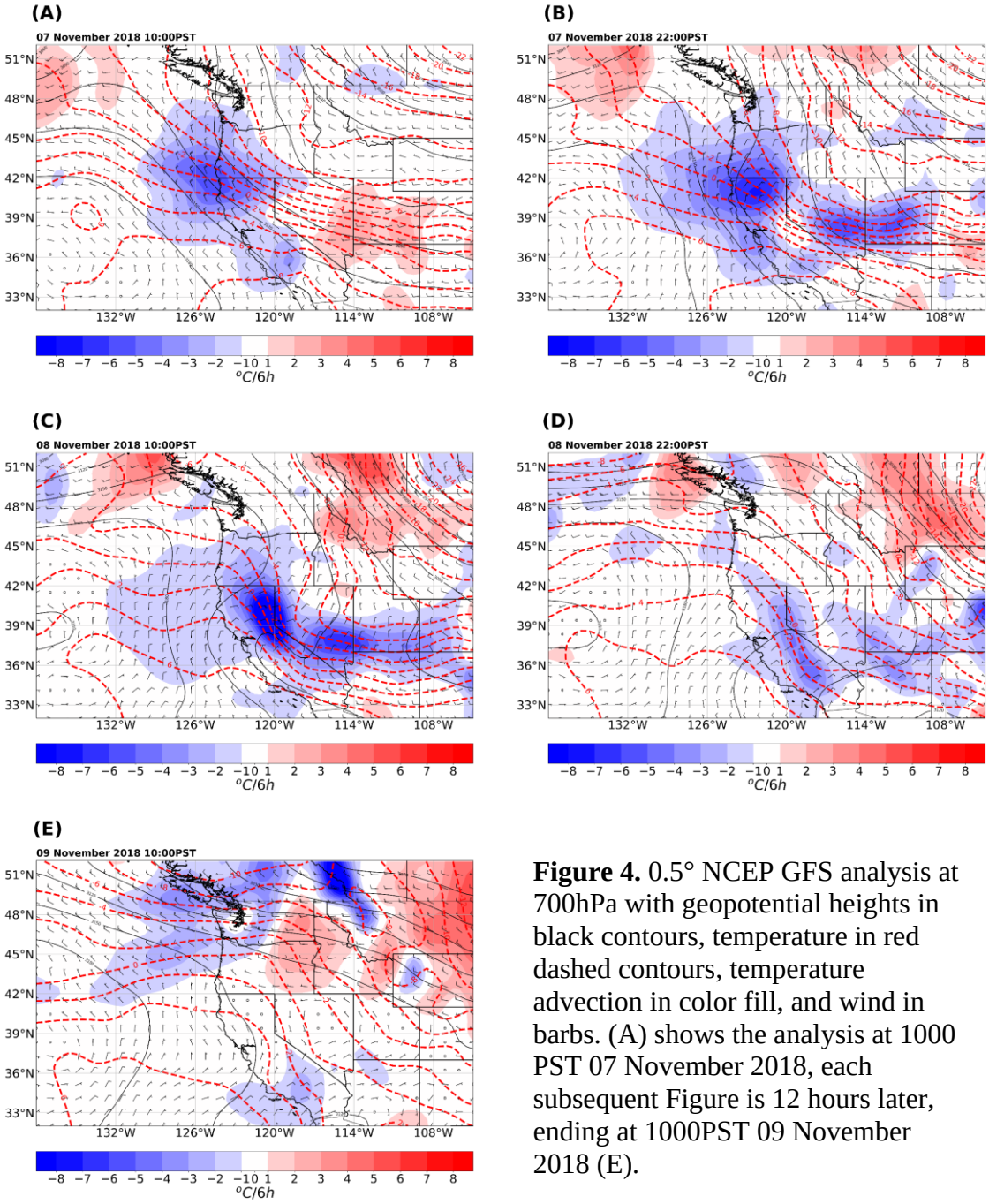

Figure 4. 0.5° NCEP GFS analysis at 700hPa with geopotential heights in black contours, temperature in red dashed contours, temperature advection in color fill, and wind in barbs. (A) shows the analysis at 1000 PST 07 November 2018, each subsequent Figure is 12 hours later, ending at 1000PST 09 November 2018 (E).

This cross-barrier flow of 7–10 m s^{-1}, roughly at crest height, is one of the basic requirements that leads to downslope windstorms. An inversion located roughly near crest top is shown in the 12:00 UTC 8 November 2018 NWS Reno, NV sounding, which indicates the last basic requirement for downslope windstorms to occur (Figure 5).

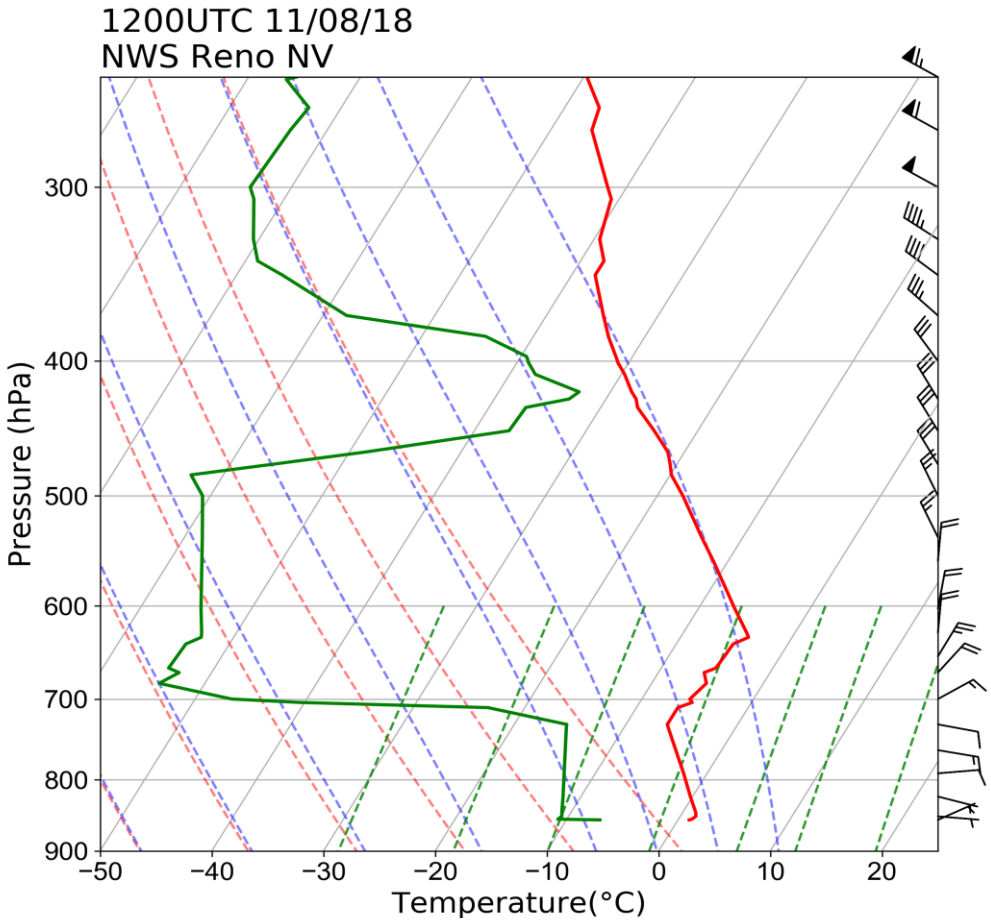

Figure 5. NWS Reno Nevada 1200 UTC 08 November 2018 Sounding.

The combination of these conditions likely led to the strong, gusty winds of >20 m s^{-1} experienced throughout much of the western slopes of the Sierra Nevada. At the surface, an inverted trough provided additional forcing, enhancing the downslope winds (Figure

6). GFS MSLP for 04:00 PST 8 November 2018–10:00 PST 9 November 2018 are shown in Figure 6A–E.

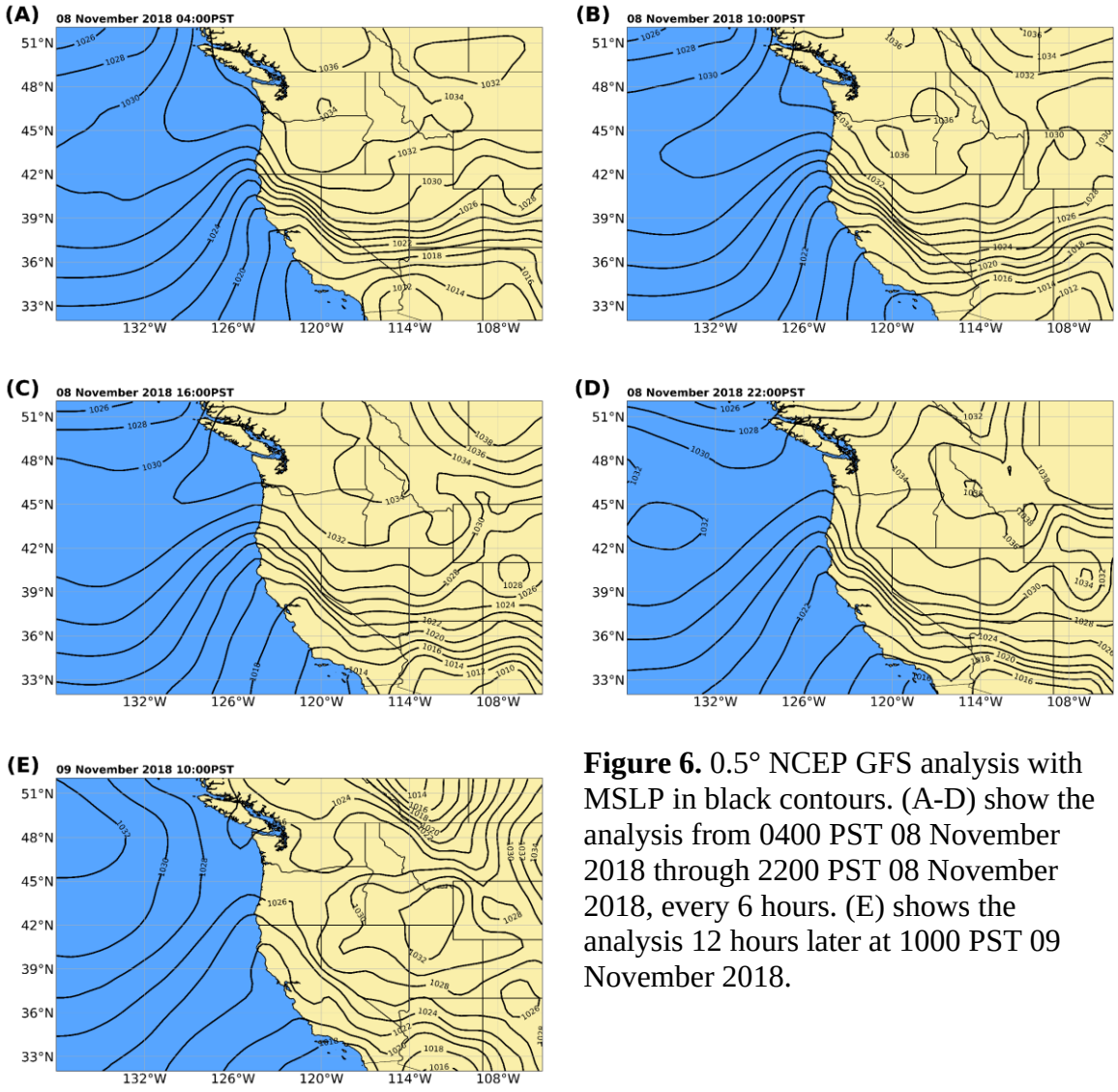

Figure 6. 0.5° NCEP GFS analysis with MSLP in black contours. (A-D) show the analysis from 0400 PST 08 November 2018 through 2200 PST 08 November 2018, every 6 hours. (E) shows the analysis 12 hours later at 1000 PST 09 November 2018.

The large pressure gradient between the surface high in eastern Oregon and northern Nevada combined with the inverted surface trough in the Central Valley of California, acted to increase near-surface wind speeds, especially in areas where gap flow occurred through mountain passes (Figure 6A). The Feather River Canyon likely funneled these

gap winds, similar to that experienced during SAW events in southern California (Raphael 2003; Edinger et al. 1964). The strong flow down the canyon was exacerbated by the already high winds associated with the synoptic-scale forced winds. The strong pressure gradient was persistent throughout the day on 8 November 2018 and into the evening (Figure 6C, D). However, aloft at 700 hPa, the geopotential height gradient, winds, and CAA continued to weaken throughout the night on 8 November 2018 as the shortwave and AWB crest continued to propagate southeast across the southwest US (Figure 4D). By the morning of 9 November 2018, the pressure gradient at the surface weakened considerably, while aloft the winds became calm–~5 m s^{-1} with flow roughly parallel with the Sierra Nevada crest (Figures 4E and 6E). On 9 November 2018, the large-scale weather pattern, which was forcing the downslope windstorm, had subsided and caused the surface winds to weaken.

Section 3.3: Observations

In situ weather observations in the area of the Camp Fire were made primarily from various surface weather stations within a roughly 60 km radius from Paradise, CA (Figure 1B, Table 1). The Jarbo Gap RAWS (Figure 7A) typically experiences moderate NE drainage winds at night and weak WSW upslope flow during the daytime, which is likely caused by local topography of the Feather River Canyon and the Sierra Nevada. However, due to the synoptically forced downslope gap winds, the station experienced very strong NE winds throughout the night of 7 November 2018 and into the morning on 8 November 2018, with sustained winds over 12 m s^{-1} and gusts over 23 m s^{-1}. During the day on 8 November 2018, the winds were moderate with sustained winds between 3–8 m

s^{-1} and gusts up to ~15 m s^{-1}. Wind speed and gusts increased in magnitude into the evening of the 8th and were steady into the morning of the 9th.

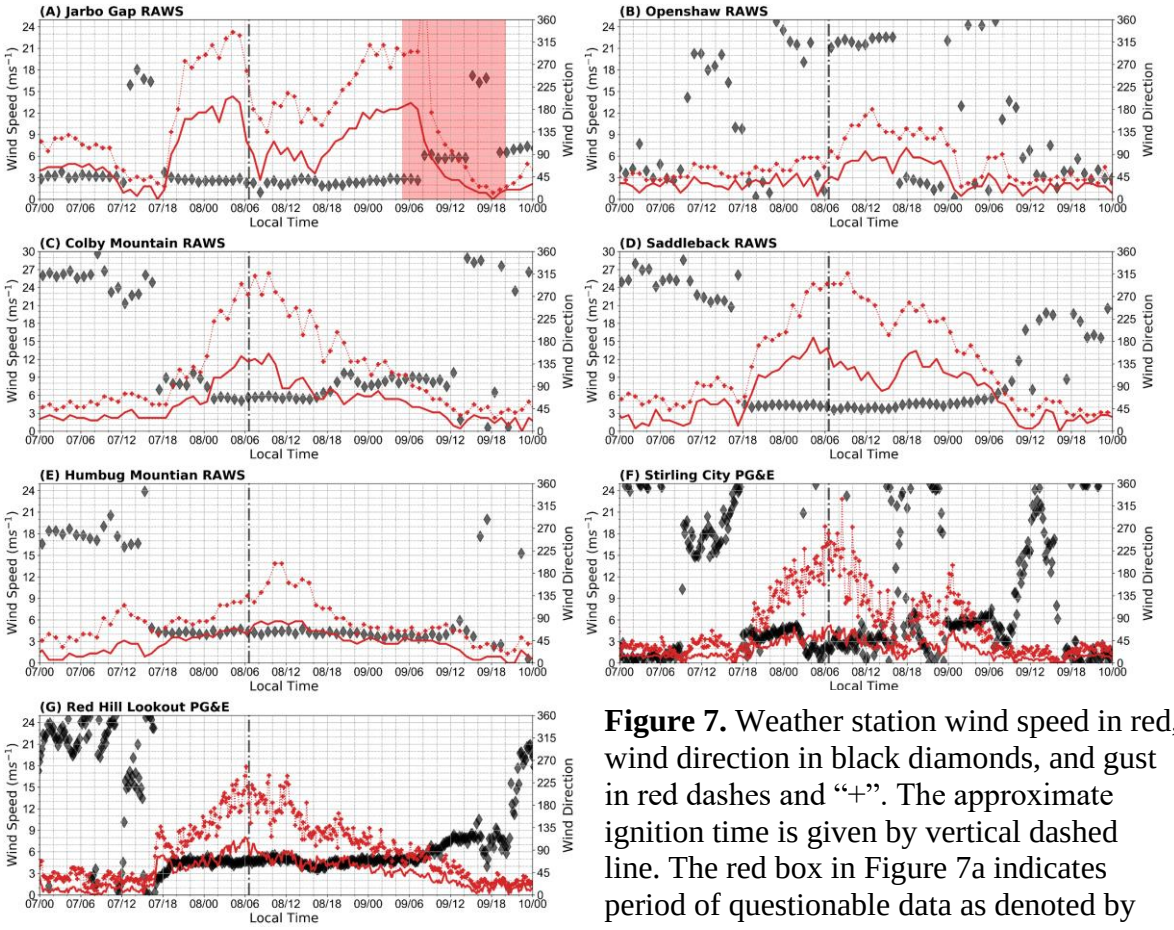

Figure 7. Weather station wind speed in red, wind direction in black diamonds, and gust in red dashes and "+". The approximate ignition time is given by vertical dashed line. The red box in Figure 7a indicates period of questionable data as denoted by Mesowest.

After 06:00 PST 9 november 2018, the data at Jarbo Gap became questionable, based off observations of soil temperature >40°C and erratic winds we believe that the station may have been burnt over or fire was very close in the time period near 08:00 PST. However, the station did record the daytime winds switching to the WNW weak upslope that would be expected with a lack of synoptic forcing influencing the winds. The Openshaw RAWS

(Figure 7B), which is located in the California Central Valley, experienced strong NW flow, with gusts of ~13 m s^{-1}, likely caused by the strong inverted surface trough. At 17:00 PST 8 November 2018, the wind direction switched to NNE with gusts of ~10 m s^{-1}, suggesting that the downslope winds were able to push farther down the slope and into the valley. The strong downslope winds that pushed into the valley were likely a factor that allowed the fire to progress to and even cross CA Highway 99, a wide four-lane highway (Figure 1B and (Camp Fire 2018)). Colby Mountain, Humbug Summit, and Saddleback RAWS all experienced similar downslope windstorm conditions, with NE and ENE winds and peak gusts occurring in late morning of the 8th. Both Colby Mountain and Saddleback RAWS recorded gusts >26 m s^{-1} with early sustained winds >10 m s^{-1}. Humbug Mountain RAWS did not experience as strong of winds, with gusts of ~14 m s^{-1} and sustained winds of ~5 m s^{-1}, but these data still indicate the presence of downslope winds. The Red Hill Lookout PG&E station observed similar conditions to that of Humbug Mountain, with ENE wind direction and extremely steady sustained winds of ~6 m s^{-1}, which began to taper off at 00:00 PST 9 November 2018. This station experienced strong gusts peaking at 18 m s^{-1} roughly at the time of ignition and tapering off similar to the sustained winds. The Stirling City PG&E station observed the strong ENE–NNE downslope winds throughout the night and morning on 8 November 2018. However, after 12:00 PST 8 November, the winds weakened and became more variable. The station experienced two periods of weak SE flow followed by stronger NNE winds, which may indicate that this station was located either underneath a rotor in the downslope winds or is poorly sited. The deployment of the CSU-MAPS truck to the

Camp Fire allowed for observations of the vertical structure of the wind. Figure 1B shows the two lidar scanning locations, which at the scan times, were approximately along the southern flank of the fire. Vertical wind profiles from the lidar are shown in Figure 8. Figure 8A shows what appears to be an intermittent low-level jet located just above the surface between 100–400 m AGL, with a separate wind maximum between 400–700 m AGL. The wind direction at the surface was northeasterly, which tended to veer eastward with height (Figure 8A). At the second scan location, Figure 8B, the winds were stronger throughout the profiles and the wind speeds tended to increase with height. Again, in this profile, the wind directions veered with height from NNE to E.

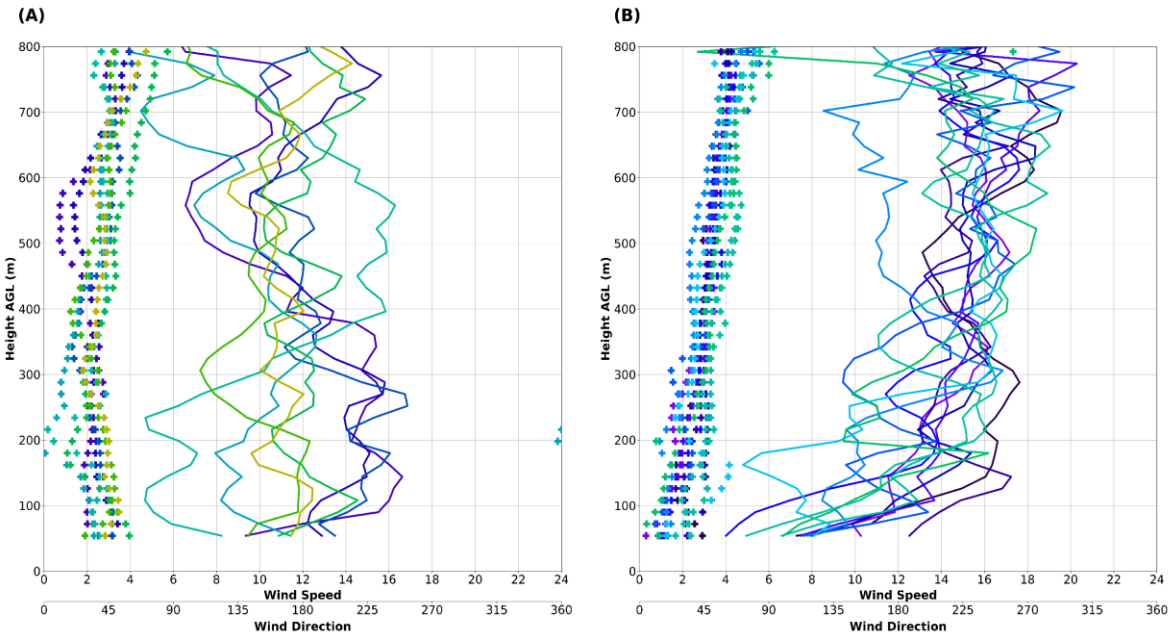

Figure 8. (A) Observed lidar vertical wind profiles from scan location #1 (Figure 1b). Wind speed is represented by the solid lines with "+" representing the corresponding wind direction. Each color represents the profile taken every 5 minutes between 1900–1940 PST 08 November 2018. (B) Lidar vertical wind profiles from scan location #2 (Figure 1b). Wind speed is represented by the solid line with "+" representing associated wind direction. Each color represents the profile taken every 5 minutes between 2100–2200 PST 08 November 2018.

Both sets of profiles show moderate winds, on the order of ~8 m s^{-1}, located just above the surface with lidar-observed boundary-layer heights of 800−1000 m AGL (not shown). These winds aloft continued to allow for the transport of firebrands in addition to increasing ROS along ridgelines and hilltops in the lower foothills to the southwest of Paradise. It should be noted that the surface winds, at the time the wind profiles were made, were weaker and so while winds at the surface were not very strong, the winds aloft were. The winds aloft mixed down to the surface bringing higher momentum from aloft to the surface, which also helped drive ember transport.

Section 3.4: WRF Analysis

Radar observations of the smoke plume were available due to the proximity of the KBBX radar. Figure 9A–E shows the evolution of both the fire and the surface winds using the base radar reflectivity and the 2 km resolution WRF 10 m winds. The 07:21 PST 8 November 2018 radar scan (Figure 9A) was the first scan time that the smoke plume became visible within the ground clutter. The next scan (Figure 9B) at 07:46 PST 8 November 2018 clearly shows the smoke plume boundaries in the reflectivity, which was aligned NE with the strong model winds. By 11:27 PST 8 November 2018 (Figure 9C), the large ash and smoke particles extended ~70 km from the base of the plume. The plume axis was still in line with the NE downslope winds, even as the plume extended over the NW surface flow in the Central Valley. Additionally, the reflectivity origin in the area of Paradise, CA resembled what may have been the fire front structure. This shape is similar to many wind-driven fire fronts with the center of the fire being spread

faster as a head fire by the wind than the flanks, thus creating an elongated “U” shape in the reflectivity (e.g., (Albini 1978; Cheney and Gould 1995)). This feature in the reflectivity persisted throughout much of the day. Figure 9D shows another example of this reflectivity structure and how the modeled winds are aligned with the plume and estimated fire front structure.

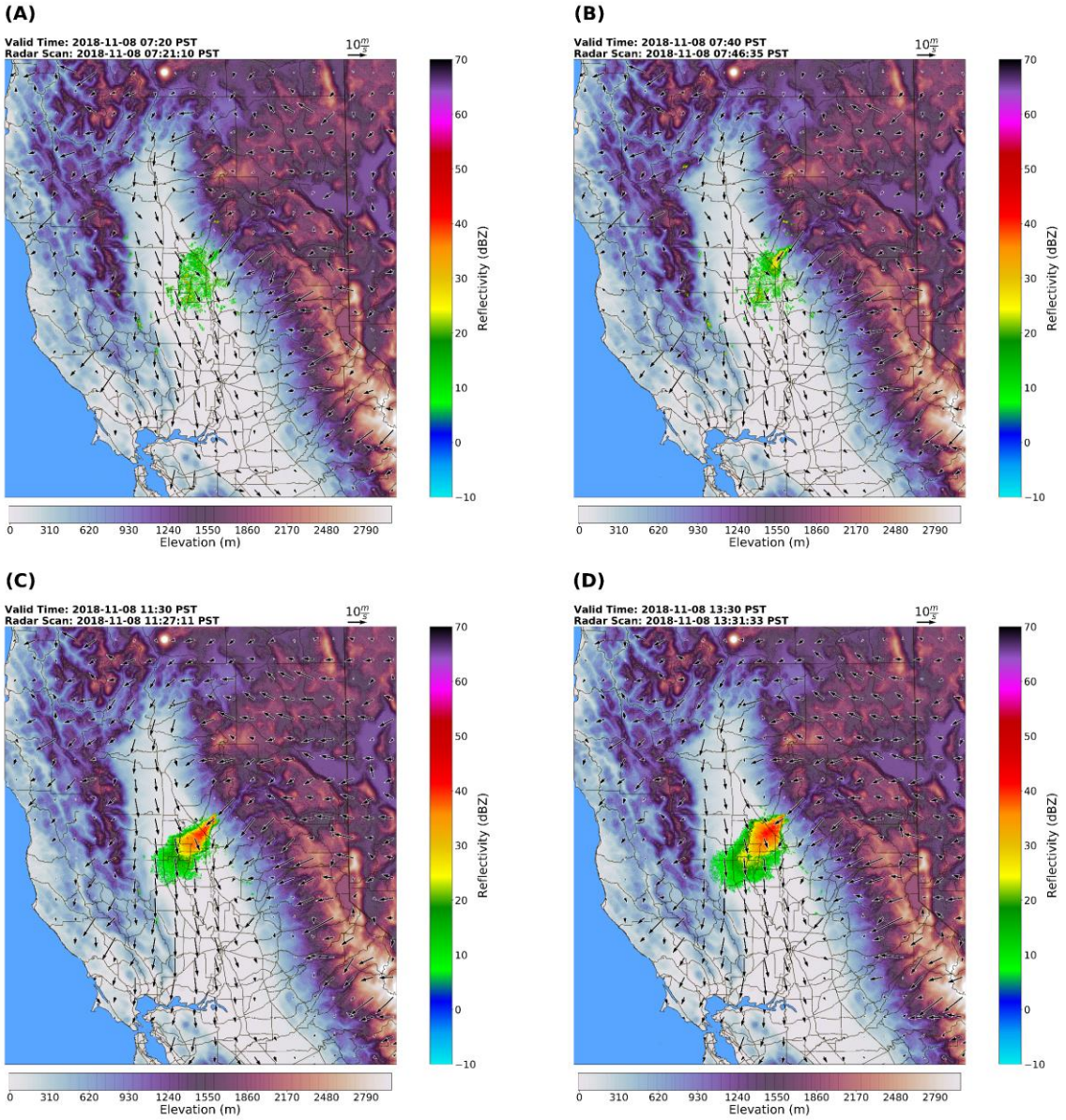

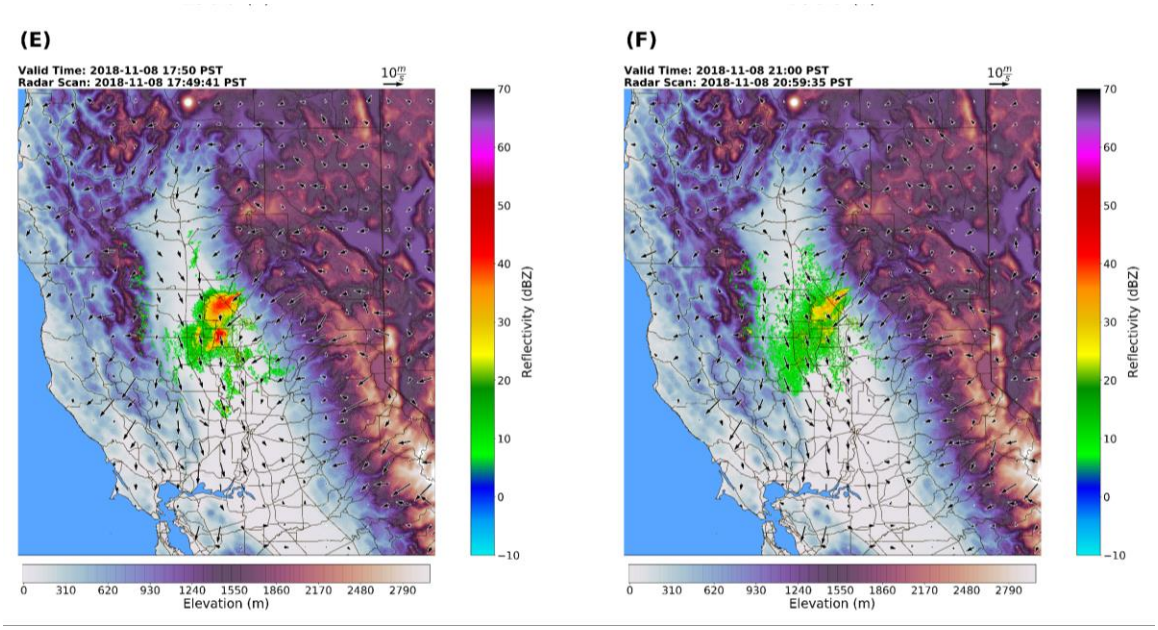

Figure 9. KBBX radar base reflectivity, WRF D2 terrain and 10m winds (vectors). Radar scan times are plotted with the nearest WRF output times of 0720, 0740, 1130, 1330,1750 and 2100 PST 08 November 2018 for subplot A, B, C, D, E, & F respectively.

As the fire continued to burn into the evening on 8 November 2018 (Figure 9E,F), the smoke plume boundaries became wider as the fire's flanks continued to burn outward, however the "U" shape in the fire front structure was still somewhat apparent. Additionally, the highest reflectivity in the smoke was coming from the area of Paradise, CA and was likely due to more ash particles and larger debris associated with many structure fires. In addition to using WRF to show the spatial extent of surface winds, cross sections of simulated wind and potential temperature were used to investigate the vertical structure of the winds and flow pattern associated with the downslope windstorm. At roughly the time of ignition, sustained winds above the surface and near the ignition point in Concow, CA were >25 m s^{-1} (Figure 10A). Additionally, Figure 10 illustrates typical flow for a downslope windstorm with the subcritical flow upstream of the crest,

which becomes supercritical accelerating down the lee of the Sierra Nevada creating multiple hydraulic jump structures (Durran 1990; Cao 2015).

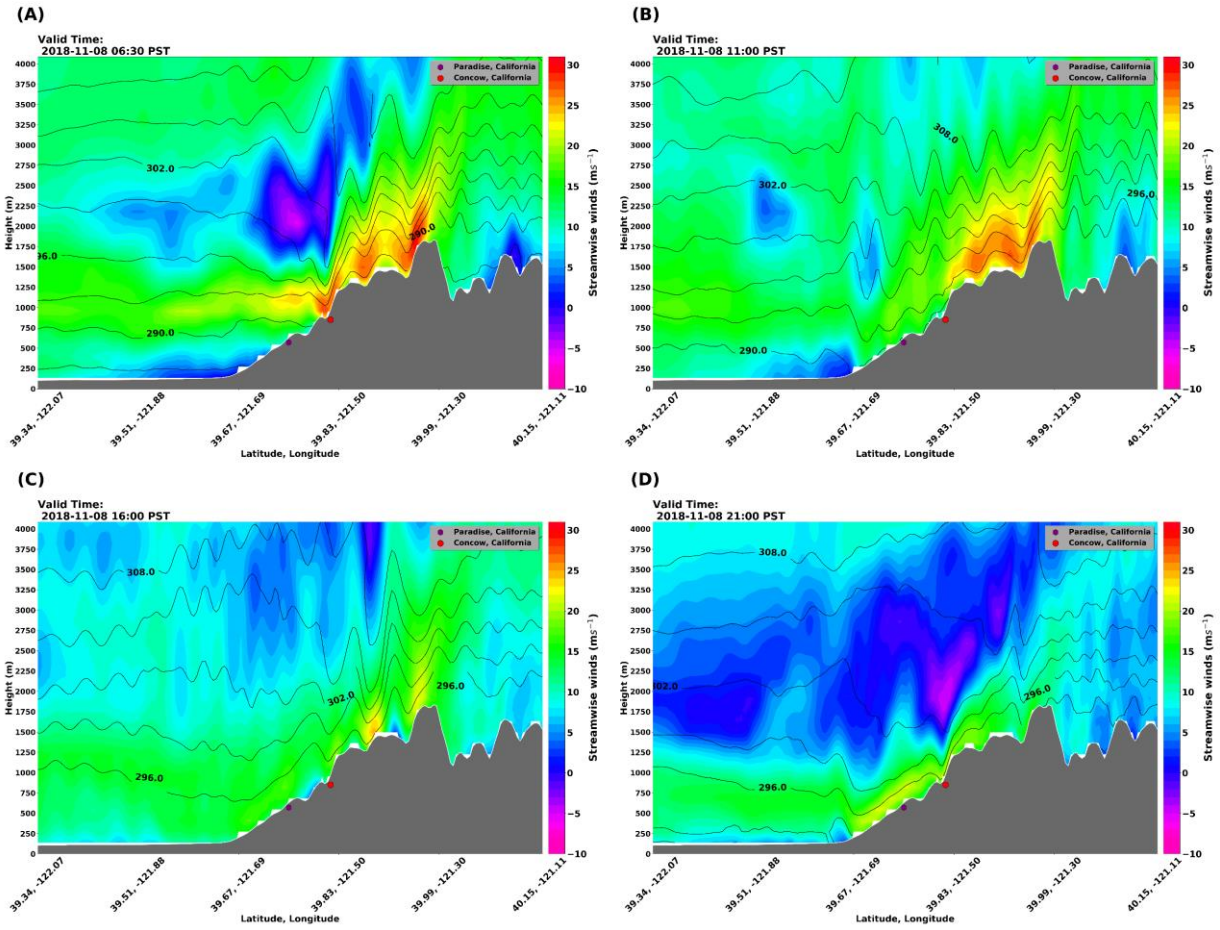

Figure 10. WRF D3, 0.666 km resolution vertical cross sections of streamwise winds (shaded), and potential temperature (contours) at 0630, 1100,1600, and 2100 PST 08 November 2018, subplots A, B, C, and D respectively. The approximate locations of Paradise (hexagon) and Concow (circle) are also shown

The synoptic features discussed above, in addition to the surface observations, suggest that this simulated downslope windstorm is realistic. The strongest winds had a tendency to stay in the higher elevations near the crest, but winds of 10–20 m s^{-1} just above the surface were present throughout much of the day in the area of Concow and Paradise

(Figure 10B,C). The downslope winds continued into the evening of 8 November 2018 as shown in Figure 10D, however as mid-level support waned, the winds likely were driven by nocturnal drainage flow combined with the pressure gradient between the Great Basin and the Central Valley. The combination of output from operational atmospheric models, surface observations, observed vertical wind profiles, and this WRF simulation, show that the strong winds associated with the Camp Fire were likely caused by a downslope windstorm and gap-flow winds. Additionally, these strong winds combined with extremely low fuel moistures created a very dangerous environment that was primed for extreme fire behavior.

Section 4: Model verification

In order to assess how WRF simulated the real atmosphere, we compared point forecasts for all weather stations used in this analysis, as well as vertical wind profiles analyzed, against our lidar vertical wind profile observations. Figure 11 gives all stations wind speed and direction compared to WRF wind speed and direction averaged over the hour period. WRF modeled winds for each station were pulled from the grid box in which each station was located. The model both overestimated and underestimated winds at many of the locations. However, at the Stirling City station, the model performed very poorly with averaged root mean square error (RMSE) of 6.77 m s^{-1}. Additionally, the model did not perform well forecasting wind direction at the Openshaw RAWS site. The model resolved NE downslope winds reaching the Openshaw station much earlier than what was observed. The RMSE wind speed and wind direction for all sites examined were 3.34 m s^{-1} and 54°, respectively. If the worst wind speed site, Stirling City, was

removed, the RMSE would drop to 2.78 m s^{-1}, and if the worst wind direction site, Openshaw, was removed, the RMSE would decrease to 35°.

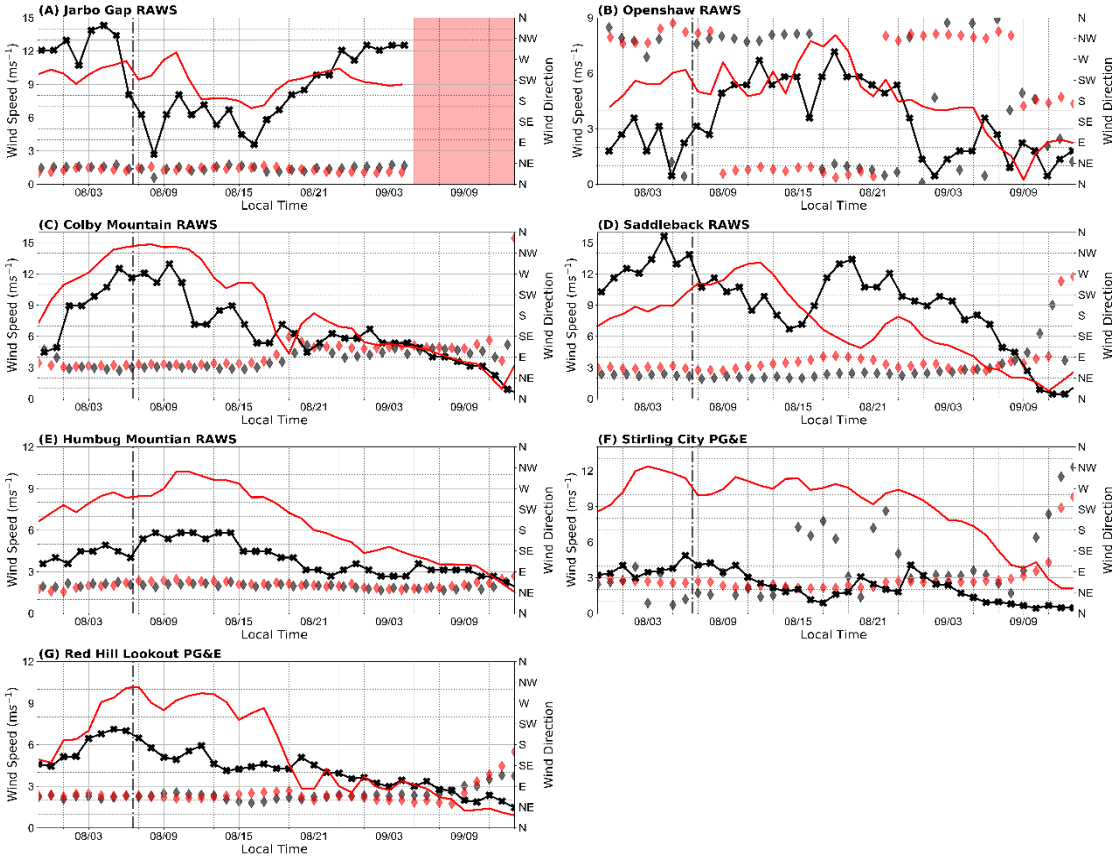

Figure 11. WRF 10m wind speed and direction, red line and diamonds; and observed wind speed and direction, black line with Xs and diamonds. Dashed vertical line indicates approximate ignition time of the fire, and the red box in subplot a.) indicates where the station data is questionable and therefore omitted.

Overall, station observations versus WRF winds showed the simulation had a high bias compared to observations from both RAWS and PG&E stations, which may be caused by station siting, terrain influence, or measurement height differences (Figure 12). Furthermore, when comparing the RAWS against the model, the majority of points are above the 1:1 line, especially with regards to lower wind speeds (Figure 12A).

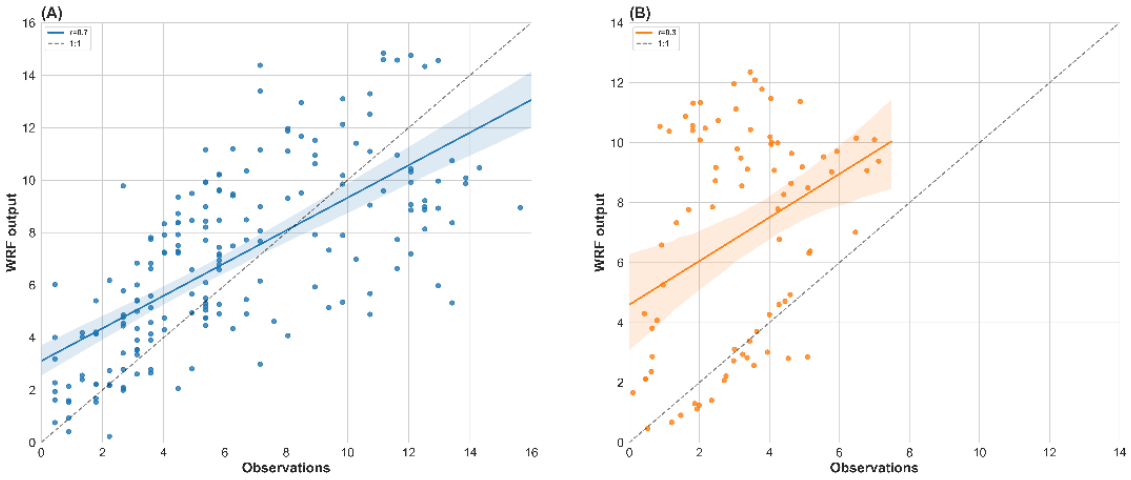

Figure 12. (A) WRF 10m winds against RAWS stations, solid blue line indicates regression line and a 95% confidence interval (shaded), dotted line indicates 1:1. (B) WRF 10m against Stirling City and Red Hill Lookout PG&E stations with regression line and confidence interval in orange

However, there is much more spread in the wind speeds above 8 m s^{-1}. When comparing the PG&E stations to the model, there is a larger high bias (Figure 12B). Much of this high bias is likely from the Stirling City station, as well as the morning and midday of 8 November 2018 periods at Red Hill Lookout. However, the grouping of well modeled winds can be attributed to the evening of 8 November 2018 and the morning of 9 November 2018 at Red Hill Lookout (Figures 11G and 12B). Our WRF simulation made reasonable forecasts of the strong winds for the RAWS stations but failed at forecasting winds at PG&E stations.

In addition to the verification against surface stations, vertical lidar wind profiles were compared to WRF vertical wind profiles to assess how well the downslope winds aloft were simulated. Figure 13 shows the comparison of the two lidar scanning locations to the vertical profile of the nearest model grid location. The averaged modeled vertical

profile and the averaged lidar wind profile were used to calculate RMSE. For both profiles, the model did not perform well. At location 1, the RMSE between modeled and observed wind speeds was 8.7 m s^{-1}. Additionally, the modeled and observed wind direction RMSE was 31.5°. The model predicted the wind direction well near the surface but resolved the shift in direction, from NE to E, at lower altitudes than what was observed. Lidar location 2 had a smaller RMSE of 4.77 m s^{-1}, which was likely due to the successful modeling of winds above 700 m AGL. The simulated wind direction at this location was also better with a RMSE of 16°. The wind profile at location 2 was simulated to be much closer to the observations with the model being able to better simulate both the change in wind direction with height and the wind speed profile. However, for both locations, the modeled wind direction had an easterly bias as compared to the observations

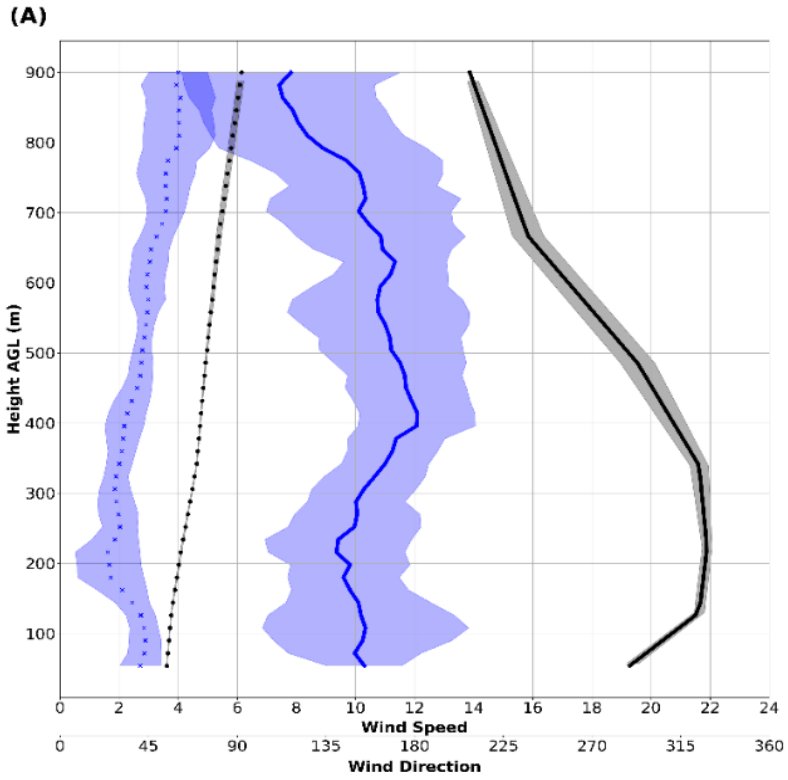

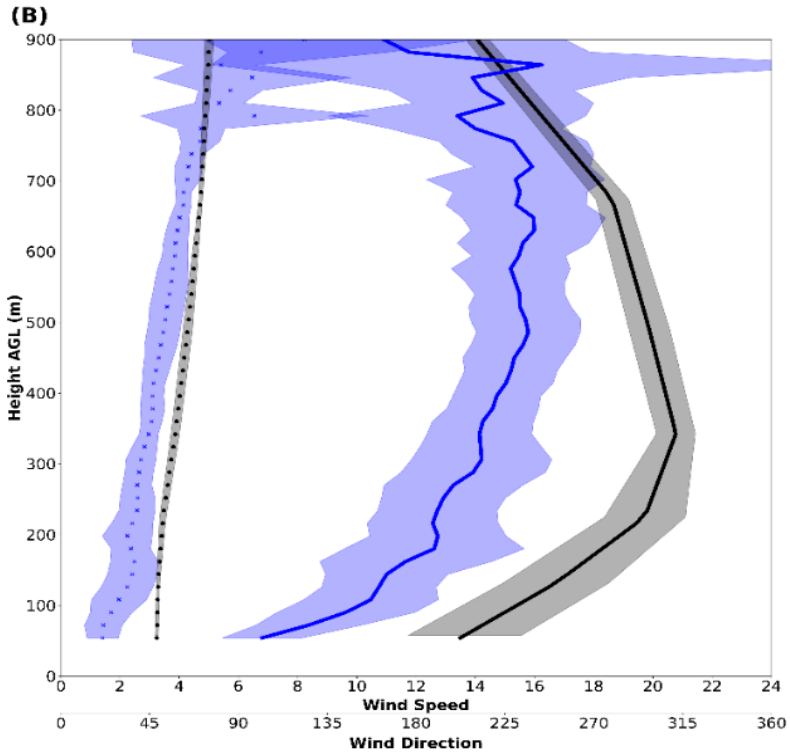

Figure 13. (A) Location #1 averaged lidar vertical wind speed (blue line) and direction (blue Xs). WRF modeled vertical wind speed (black line) and direction (black circles). Shading indicates ± 1 standard deviation. (B) Location #2 averaged lidar vertical wind speed (blue line) and direction (blue Xs). WRF modeled vertical wind speed (black line) and direction (black circles). Shading indicates ± 1 standard deviation.

Section 5: Discussion and Conclusions

The 2018 Camp Fire occurred during an episode of high-risk fire weather conditions. The lack of precipitation in the months leading up to ignition created an environment where calculated dead and live fuel moistures reached their record minimum. This environment alone had the potential to carry fire in the event of an ignition. The onset of a downslope windstorm from the evening on 7 November 2018 through the morning of 9 November 2018 created more critical conditions allowing for more rapid rates of spread, which caused the Camp Fire to be a fast moving and deadly wildfire event. A combination of synoptic events led to the development of the strong

downslope windstorm. These events included the evolution of the mid-level atmosphere, which was caused by CAA potentially initiating and deepening a shortwave trough embedded within a high amplitude ridge. The amplified shortwave created flow perpendicular to the Sierra Nevada crest, and in addition to the presence of an upstream temperature inversion at crest level, provided the conditions needed for downslope windstorm development. Furthermore, surface pressure gradients throughout 8 November 2018 likely exacerbated the strong downslope winds. The pressure gradient between the California Central Valley and the Great Basin allowed for strong gap flow. This gap flow was particularly evident in the Feather River Canyon which recorded gusts of ~23 m s^{-1}. The synoptic-scale meteorological patterns associated with this event were similar to both DW and SAW events, but North wind events in the northern Sierra Nevada have, to date, not been thoroughly researched. Prediction of these windstorms is important for assessing fire danger especially for utility companies and preplanning for at-risk communities in the Sierra Nevada.

Observations from surface weather stations showed the presence of downslope winds associated with the event. RAWS and PG&E stations located near the Camp Fire recorded moderate to strong sustained winds between 5–15 m s^{-1} and gusts greater than 26 m s^{-1} during the first day of the fire, 8 November 2018. These winds were predominantly out of the NNE–E, indicative of typical downslope windstorms in the region. Doppler lidar observations made in the evening of 8 November 2018 indicated the presence of nearly constant and strong winds throughout the boundary layer, which were NE near the surface and veered with height to easterly aloft. The vertical wind profiles

also indicated the presence of an elevated low-level jet structure intermittently. In addition to the to the Doppler lidar observations, radar reflectivity of the smoke plume on 8 November 2018, indicated the wind-driven nature of the fire front and that the smoke plume was aligned from NE to SW along the predominant downslope wind direction. Observations in this study were able to verify that a downslope windstorm occurred. However, an increase in observations, both well-sited weather stations as well as lidar profilers, would be beneficial in providing real-time updates on the onset of these windstorms. Knowing when the onset of the strong wind occurs may be useful for utilities and local fire managers to be better prepared for future large wildfire events.

WRF simulations provided added context to the observations. For example, the simulations indicated that the vertical structure of the atmosphere throughout 8 November 2018 was indicative of a downslope windstorm. The simulated vertical cross sections of streamwise winds and potential temperature showed the presence of subcritical flow upstream of the ridgeline, which transitioned to the supercritical flow. The strongest winds in the simulation tended to be confined to higher elevations, but winds of over 20 m s^{-1} were not uncommon in areas further down the slope from Concow and Paradise. Additionally, the simulations revealed the presence of many hydraulic jump structures within the downslope windstorm, which may explain some of the observations of erratic winds at the Stirling City PG&E surface station. Furthermore, the hydraulic jump structures may be linked to intermittent gusty winds experienced on the ground and the lofting of fire brands during the fire.

Model performance when compared to observations varied. When compared to surface station observations, the model performed reasonably well with a strong correlation with RAWS, but an overall high bias was associated with weaker observed winds. When compared to the two PG&E stations, WRF performed poorly. The PG&E stations are not standardized, with instruments mounted at various heights with no information on heights or station placement. Due to the unknown placement of these sites and instruments, it is possible that the site is in an obstructed area or much closer to the ground than assumed. Additionally, due to the resolution of the model, there may have been subgrid-scale processes, such as lee-side rotors, that were not resolved in the simulations. Moreover, complex terrain may not be well resolved within the model, which may also affect how winds are simulated. When compared to lidar observed vertical wind profiles, WRF again had a high wind speed bias. This bias may be caused by the PBL parameterization resolving a characteristic log-wind profile that differed from the actual observations. These biases in WRF can be used by forecasters and fire managers to be able to better assess what the winds are doing on the ground, especially if they are utilizing a mesoscale forecasting model, such as WRF.

The 2018 Camp Fire event was one of the most devastating wildfires in California history. This event represents a case of extreme fire behavior associated with critically dry fuels and the onset of a downslope windstorm. The synoptic-scale meteorological conditions were well forecasted, and the severity of the event was not surprising given the fire danger potential for that day. We show that our rapid-response deployment to that event provided a unique dataset not available through standard surface

networks and that these data are necessary to evaluate the meteorological conditions at the fire front. However, our study does have some limitations that need to be mentioned. One limitation of this study is that we do not describe the fire behavior in detail but focus primarily on the meteorological factors associated with the event rather than the fire evolution. Another caveat to our study is that we do not know how the atmosphere responded to the fire and whether or not our observed wind profiles were impacted by fire-induced circulations that may have formed in response to fire front heating. Finally, we want to point out that fire management operations may indeed benefit from the use of wind profilers, such as Doppler lidars, to better understand the evolution of downslope windstorms and other fire weather phenomena that are poorly understood and observed.

Chapter 2

Meteorological Profiling in the Fire Environment Using UAS

Section 1: Introduction

It is well known that the atmosphere influences many aspects of wildfire behavior and that the fire itself influences the atmosphere. A number of studies, such as Byram (1954); Garcia Diez et al. (1994); and Potter (1996), made qualitative correlations between ambient weather variables, such as wind speed and relative humidity (RH), and fire behavior. These studies used vertical profiles of atmospheric parameters to qualitatively predict how the atmosphere affects fire behavior (Byram 1954; Garcia Diez et al. 1994; Potter 1996; Haines 1988). There are several indices and metrics to quantify risk for large fires or extreme fire behavior based on atmospheric parameters. Examples of these indices include the Haines Index, Fosberg Fire Weather (FFWI), and Hot-Dry-Windy index (HDW) (Haines 1988; Fosberg 1978; Goodrick 2002; Srock et al. 2018). The Haines Index relies on upper air sounding to calculate the temperature difference between two levels and the dewpoint depression at a specific level, which gives a measure of atmospheric stability (Haines 1988). The FFWI non-linearly combines temperature, relative humidity and wind speed, with outputs ranging from 0-100 where values represent expected flame length and fuel drying (Fosberg 1978; Goodrick 2002). The HDW index combines the maximum of vapor pressure deficit (VPD), a function of temperature and RH, and wind speed in the lowest 500 m of the atmosphere to create an output that can be used to predict extreme fire weather (Srock et al. 2018). Each of these

indices attempts to quantify how specific sets of atmospheric variables affect wildfire growth, behavior, or ignition.

The above atmosphere-fire interactions generally attempt to give an indication of fire danger and behavior caused by ambient and local weather conditions. Clements and Seto (2014), Lareau and Clements (2017), and Clements et al. (2007, 2016, 2019), focused specifically on quantifying the fire induced effects on the atmosphere. FireFlux was one of the first experiments that measured the microscale meteorology and turbulence associated with a fire front (Clements et al. 2007). This study was able to measure winds induced by the fire that were 2-3 times stronger than the ambient winds, as well as strong updrafts and downdrafts (Clements et al. 2007). The FireFlux experiment became the base standard for future experimental burns that included a component focused on fire-atmosphere interactions such as RxCADRE, FireFlux II, and the Fire and Smoke Model Evaluation Experiment (FASMEE), along with various smaller burns (Clements et al. 2016, 2019; Prichard et al. 2019). An important objective of the above studies was to provide a high-quality dataset for the improvement and validation of various fire-atmosphere coupled models. Fire-atmosphere coupled models resolve or parameterize very small-scale processes which can be very difficult to measure but can have impacts on processes within the model, such as fire behavior including rate of fire spread, and smoke transport. Having a dataset of observations from many different types of fires that can be used to validate against models is important to continue to improve models and measurement techniques. However, setting up tall

meteorological towers during experimental prescribed fires is time consuming and expensive.

This cumbersome technique could be replaced by unmanned aerial systems (UAS), often referred to as unmanned aerial vehicles (UAVs) or drones, which have been used for atmospheric research as far back as 1961 (Elston et al. 2015; Houston et al. 2012; Kiefer et al. 2012). One application of UAS use for atmospheric research is measuring wind. There are two main methods are often used to estimate wind speed and direction with UAS. The direct method, as described by Palomaki et al. (2017), is measuring wind speed and direction directly using some type of anemometer mounted to the platform. The indirect method estimates the wind speed and direction based on the UAS's change in attitude measured by an inertial measurement unit (IMU) and has been extensively tested and shown to be a valid measurement technique (Palomaki et al. 2017; Chilson et al. 2019). The direct method, implemented in this project, has been tested extensively with a sonic anemometer mounted directly above the UAS platform to measure 2D winds (Palomaki et al. 2017; Barbieri et al. 2019; Shimura et al. 2018). These studies all found that the use of sonic anemometers on UAS was feasible and provided reasonable accuracy when compared to station tower measurements. The ability to replicate tower-based measurements using an UAS platform would allow for mobile and rapid deployment wind measurements at controlled prescribed wildland fires and potentially at wildfire incidents.

The use of UAS in the wildland fire environment is relatively sparse and still very restricted for several reasons. Typically, UAS has been used to remotely sense wildfires

and map their perimeters (Kiefer et al. 2012; Merino et al. 2012; Moran et al. 2019; Samiappan et al. 2019). One of the first cases of using UAS to fly into a smoke plume was done by Kiefer et al. (2012), who used a manually flown fixed wing UAS equipped with a radiosonde package. This study showed that the use of UAS at a controlled wildland fire was feasible. More recently, FASMEE laid the groundwork for additional UAS usage at large wildland fires (Prichard et al. 2019). The use of UAS at wildland fires is made complex primarily due to airspace restrictions caused by manned aircraft within the airspace. Controlled wildland fire experiments, such as FASMEE, help to alleviate this restriction by coordinating flights and maintaining close communication between manned and unmanned aircraft pilots (Prichard et al. 2019; Kiefer et al. 2012; Kobziar et al. 2019; Nelson et al. 2019). The purpose of this proof of concept study is to demonstrate the utility of UAS platforms that can be used at a controlled wildland fire to sample the vertical wind profile of 3D winds measured by multiple sonic anemometers for fire weather observations.

Section 2: Background

The motivation to build and test this platform was to have an alternative to tall tower observations. FASMEE provided an ideal opportunity to test this system. The controlled burns during FASMEE were large, > 300 ha, stand replacement crown fires, which is the closest an experimental prescribed fire can approximate a real wildfire. Due to this being a controlled fire, research UAS flights were planned into the burn operations plan with cooperation between helicopter ignition crews, the United States Forest Service (USFS), and Desert Research Institute. All UAS operations were conducted under a

Certificates of Waiver or Authorization (COA) from the FAA which allowed for flights up to 1500 feet above ground level. The COA allowed for deep vertical profiles to be taken, while integration of UAS into the burn plan allowed for UAS to operate very close to a large fire without affecting air, ground operations, and safety. In addition to taking a vertical profile with the UAS, stationary "tower" flights were planned where the UAS would hover in one location to sample the winds as a replacement for a tower.

Section 3: Methods

The platform chosen was the DJI Matrice 200 version 2 (M200) quadcopter. This commercial, off-the-shelf platform was implemented for several reasons. To allow for future use, the UAS had to be simple to fly, include obstacle avoidance measures, and be easy to maintain. Additionally, the M200 had other desirable features such as adjusting for center of gravity, increased battery life, and compatibility with thermal and multispectral cameras. The sensor used to obtain wind measurements was an Anemoment, LLC, TriSonica Mini Weather Sensor. This instrument records three components of wind speed (u, v, w), wind direction, sonic temperature, humidity, pressure, magnetic heading, pitch, and roll at rates up to 5 Hz. This sensor is ideal for UAS due to the output of magnetic heading and accelerometer corrections as well as its small mass of only 50 g. The sensor was mounted to a boom extending off the side of the UAS platform, while the data logger was fixed to the top of the UAS and was powered from a 5 V USB port integrated on the M200. We decided to mount the TriSonica on an extended boom to minimize any biases caused by rotor wash on the measurements. We

also added an additional stabilizing cross-arm to reduce boom motion. The platform is shown in Figure 14.

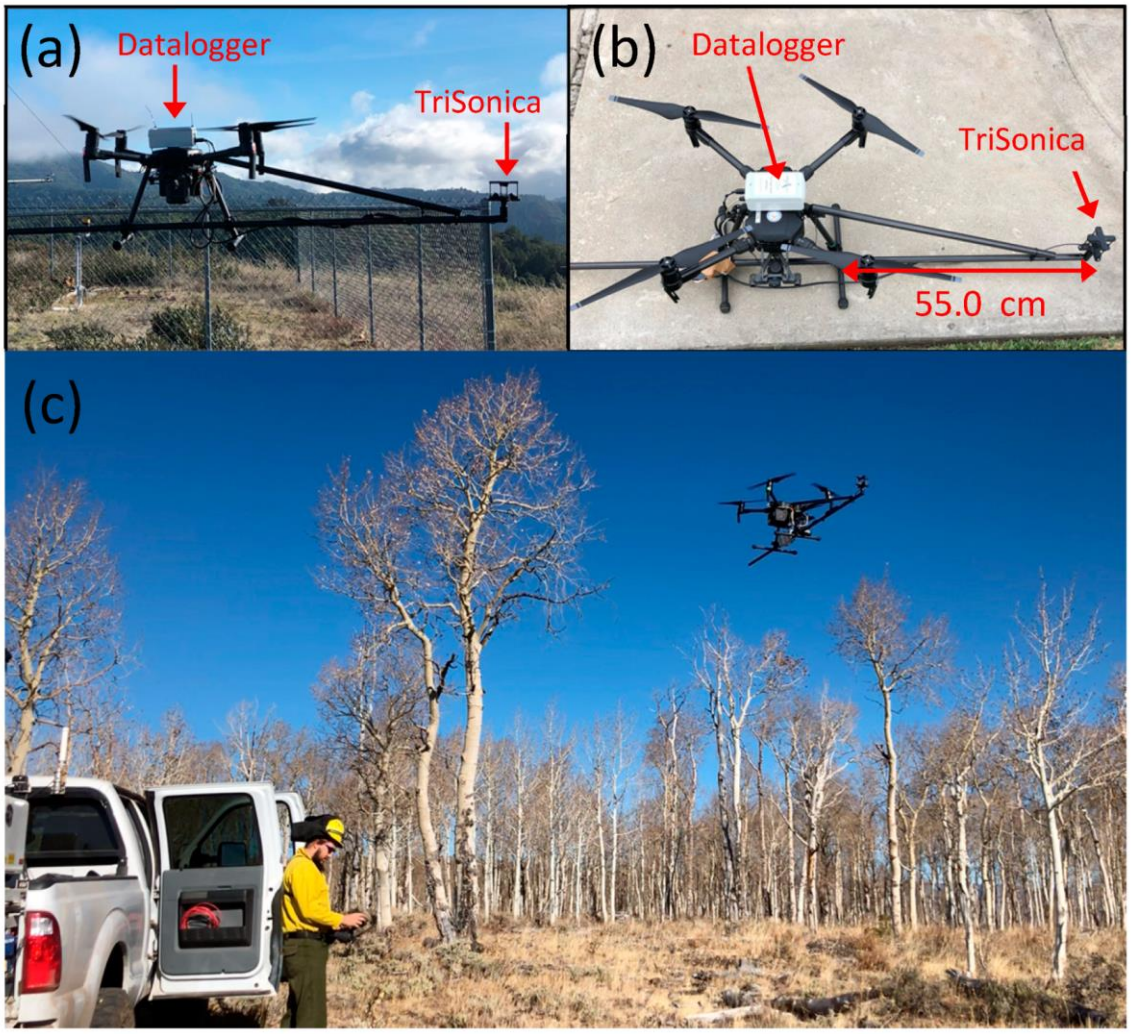

Figure 14. Photos of UAS system to showing system setup, design, and operation. (a) Horizontal view of system while hovering. (b) The TriSonica was mounted on a carbon fiber pole extending 55 cm off the body of the UAS with the data logger fixed to the top of the platform. (c) The profiling flight in the Fishlake National Forest, Utah, 7 Nov. 2019.

To test the accuracy and biases of the system we made multiple flights next to a R.M. Young (RMY) 81000 3-d sonic anemometer. The RMY anemometer measures wind velocity components (u,v,w) and sonic temperature. These data were logged using a

Campbell Scientific, Inc, CR1000 data logger at 5 Hz to match the TriSonica data. The RMY and TriSonica specifications are listed in table 3.

Table 3. Specifications of TriSonica and RMY sonic anemometers

	TriSonica	RMY
Wind Speed	Range: 0–50ms^{-1} Accuracy: (0-10ms^{-1}): ±0.1ms^{-1} Resolution: 0.1ms^{-1}	Range: 0–40ms^{-1} Accuracy: (0-30ms^{-1}): ±1% ±0.05ms^{-1} Resolution: 0.01ms^{-1}
Wind Direction	Range: 0–360° Accuracy: ±1.0° Resolution: 1.0°	Range: 0–360° Accuracy: (0-30ms^{-1}): ±2° Resolution: 0.1ms^{-1}
Sonic Temperature	Range: -40°C–80°C Accuracy: ±2°C Resolution: 0.1°	Range: -50°C–50°C Accuracy: (0-30ms-1): ±2°C Resolution: 0.01°

Test flights were performed at a remote automatic weather station operated by San José State University. The RMY sonic was mounted at 6 m AGL, and the UAS was flown at approximately the same height as the RMY. The UAS has roughly 20 minutes of flight time per set of batteries, therefore the UAS was flown into position and a 10-minute sampling period was used to ensure safe return of the platform. An additional flight was made to test how the platform preformed in low wind conditions. This test was done similarly to the above flights but used a 2m tripod to mount the RMY. The 5 Hz frequency data were averaged using 1 and 15 s moving average windows. Additionally, data were resampled to 15 s averages for scatter plot comparisons.

Section 4: Results

Section 4.1: Langdon Mountain Burn

The Langdon Mountain prescribed fire was a ~360 ha burn within the Fishlake National Forest located in central Utah conducted on 7 November 2019. The UAS access to the Langdon Mountain unit was limited, with the launch area being ~2 km away from the burn unit. Additionally, there was a limited flight window before the burn due to aerial ignition operations which persisted throughout much of the burn period. This resulted in only two flights to be made with the UAS which provided two vertical profiles. We were unable to sample during the burn, due to the ongoing aerial ignition. The first profile was flown to ~365 m AGL and the second profile was flown to ~175 m AGL, both profile ascent rates were made at 2 m s^{-1}. The soundings, plotted on a Skew-T diagram in Figure 15, show that the UAS and TriSonica weather station can make high-resolution soundings.

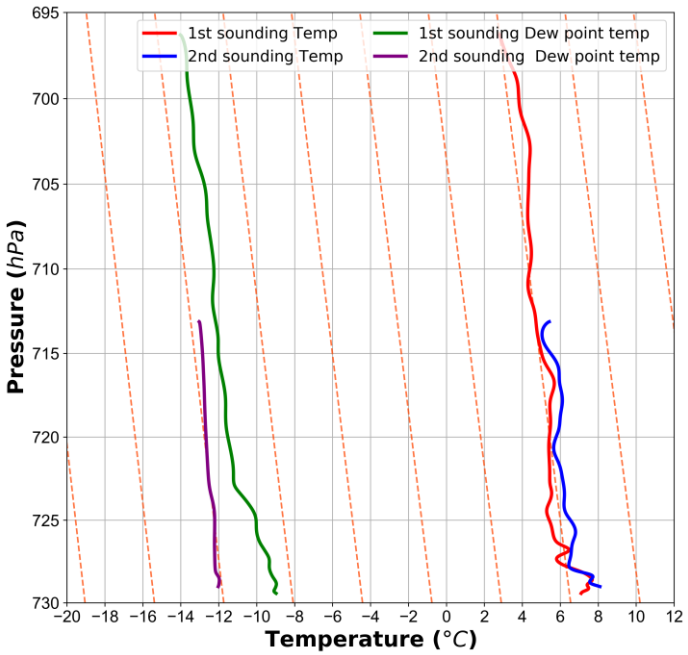

Figure 15. Skew-T logP plot of temperature and dewpoint temperature from vertical profiles taken with the UAS system prior to the Langdon Mountain burn

Above 725 hPa, the profiles were both approximately dry adiabatic. However, the sounding was able to resolve small-scale structures, such as shallow inversions just above the surface and super adiabatic layers in both profiles. In Figure 16a, the small-scale temperature structures are emphasized, the weak inversion at the surface in the sounding is roughly 10 m deep with a super adiabatic layer above.

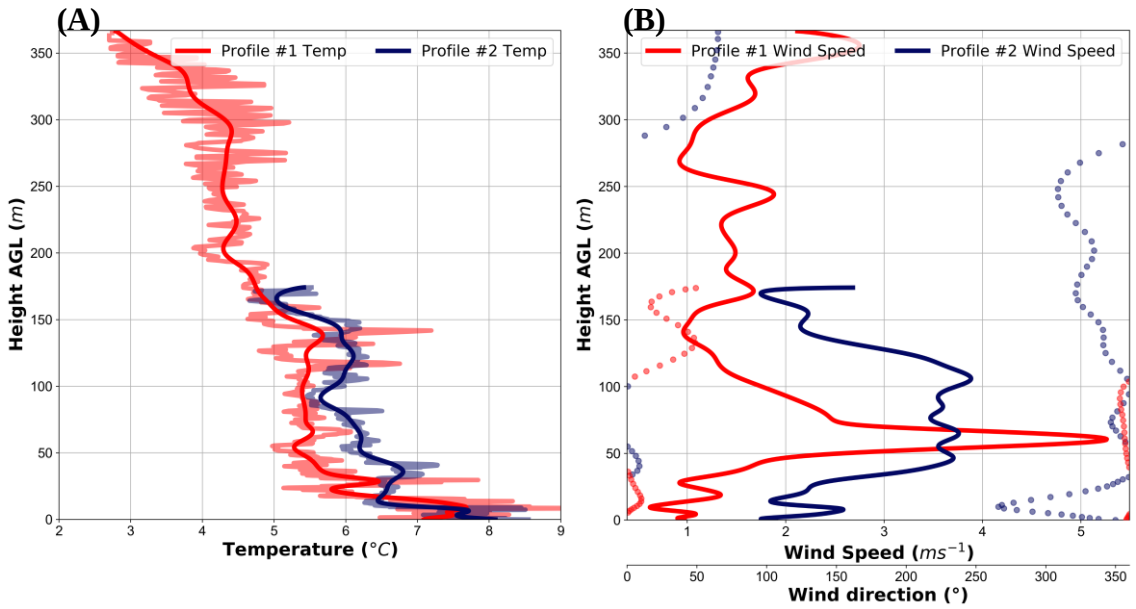

Figure 16. (A) Temperature vs height AGL for profile 1 in red and profile 2 in blue. Bold profiles indicate 15 second moving average with the semi-transparent profiles indicating 1 second moving average. (B) Wind speed in solid lines and wind direction in dot for profile 1 in red and profile 2 in blue.

The super adiabatic layer in both profiles had a lapse rate of approximately 1.5°C per 10 m. Above the super adiabatic layer at ~25 m AGL, was a ~125 m deep isothermal layer, which was observed in both profiles, was collocated with wind maximum (Figure 16b). While these "jets" were still weak, they were 2-4 m s^{-1} greater than the winds above and below. These profiles demonstrate the utility of a UAS to make high-resolution vertical atmospheric soundings within the wildland fire environment. Soundings taken close to

both controlled and wildland fires can provide valuable information about the critical winds that can influence fire behavior and provide data for various fire-weather indices, as well as how the smoke will transport and disperse.

Section 4.2: Intercomparison Study:

This section examines tests between the Trisonica and RMY anemometers, in order to evaluate the performance of the UAS system compared to fixed measurements. The tests were done with two different setups and goals. First a calm, low-wind conditions test performed using a 2 m tower in order to test for any systematic biases in the UAS based measurements caused by rotor wash. The second test case was performed to evaluate how the UAS system would perform in conditions in which the system would be replacing tower-based measurements.

Section 4.2.1: Low-Wind Comparison

In this section, the data from when the UAS was flown in a calm wind environment are examined. This flight was made to test if there are biases caused by the rotor wash and to test sensitivity of the platform. The time series of the test is shown in Figure 17. In this low wind speed test, the UAS platform performed exceptionally well when compared to the RMY. The wind speed and temperature RMSE was 0.34 m s^{-1} and 0.39°C respectively; these RMSE values are very similar to the RMSEs of 0.32 m s^{-1} and 0.42°C, when the TriSonica was mounted on the 6.1 m tower. Additionally, the 5-minute averaged wind speeds were within 0.02 m s^{-1} of each other.

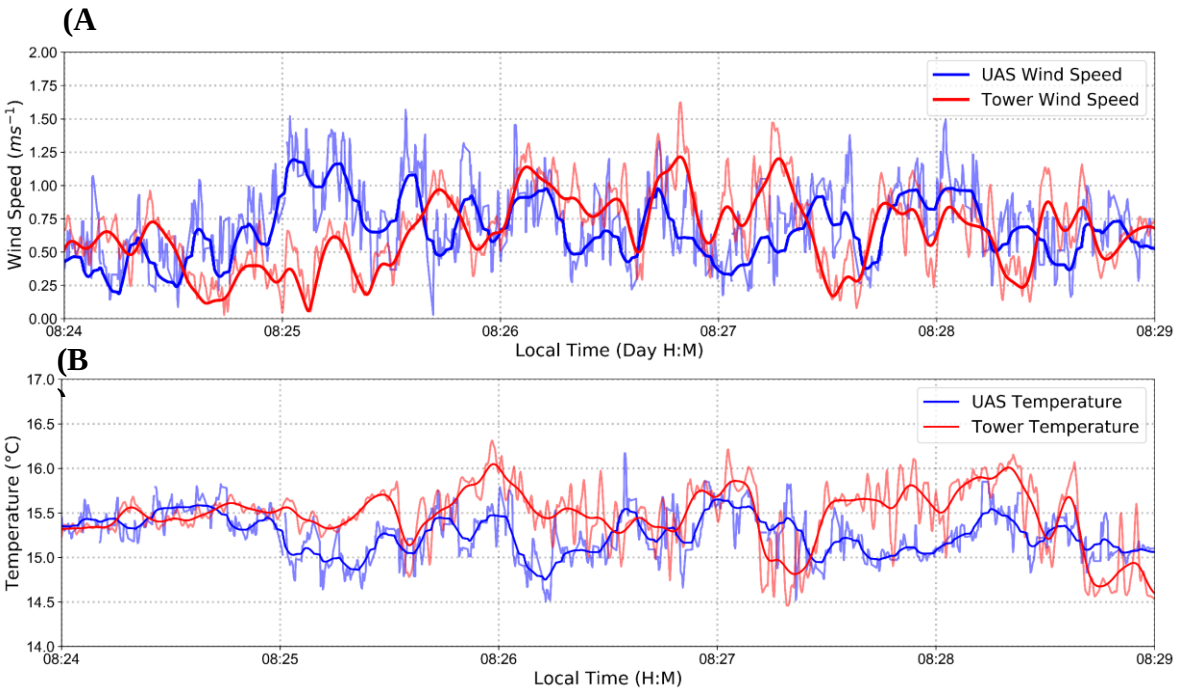

Figure 17. (A) Low-wind time series of RMY and UAS wind speed in red and blue respectively. Bold lines represent 15 second moving average with semi-transparent representing 1 second moving average. (B) Low wind time series of RMY and UAS sonic temperature in red and blue respectively with time averaging noted above.

4.2.2: Moderate-Wind Comparison

In this section, two flights will be analyzed against the RMY anemometer, as well as a comparison from when the TriSonica anemometer was mounted on the tower next to the RMY anemometer. Wind speed comparisons from both flights are shown in Figure 18. From both flights, there is an overall positive bias of ~0.5 m s^{-1} in the UAS measured wind speeds compared to the RMY tower measurements. However, this bias is not constant, with periods of UAS wind speeds 1 m s^{-1} less than tower wind speeds in both flights. When combining the two flights and plotting them against the respective tower observations, the high bias in the UAS measurements becomes clearer (Figure 18c).

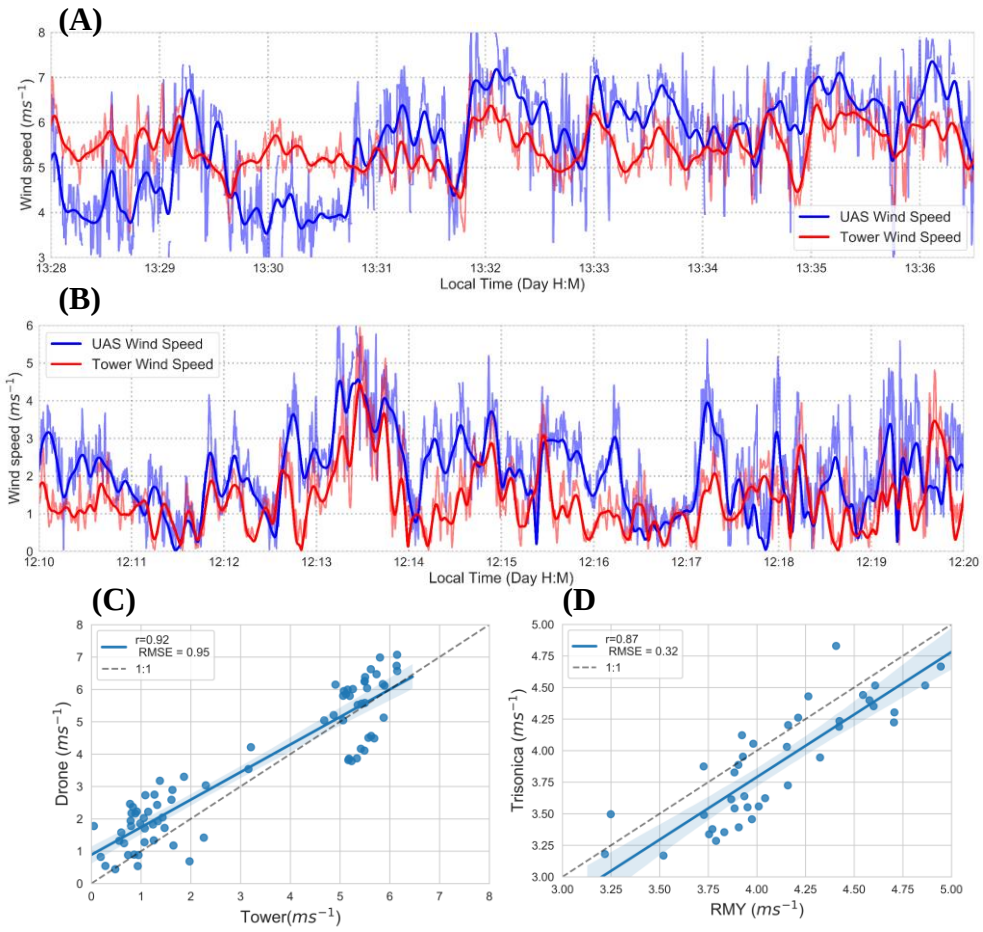

Figure 18. (A) Flight 1 time series of RMY and UAS wind speed in red and blue, respectively. Bold lines represent 15 second moving average with semi-transparent representing 1 second moving average. (B) Flight 2 time series of RMY and UAS wind speed in red and blue respectively with time averaging noted above. (C) Scatter plot of UAS wind speed versus RMY wind speeds for both flights in blue dots. Linear regression and 95% confidence interval in blue line and shading. (D) Scatter plot of tower mounted Trisonica wind speed versus RMY wind speeds in blue dots. Linear regression and 95% confidence interval in blue line and shading.

The RMSE from flight 1 (flight 2) was 0.91 m s^{-1} (1.11ms^{-1}), with a combined RMSE of 0.95 m s^{-1}. Additionally, as seen in Figure 18d, when the anemometers were mounted next to each other, the TriSonica anemometer had a low bias compared to the RMY anemometer. The averaged wind speeds from the UAS and RMY for flight 1 and flight 2 were 5.6 m s^{-1} and 5.4 m s^{-1}, and 2.0 m s^{-1} and 1.39 m s^{-1}, respectively.

The time series of sonic temperatures, Figure 19a-c, shows that the TriSonica can accurately measure temperature compared to the RMY. The RMSE from flight 1 (flight 2) was 0.28°C (0.78°C) and a combined RMSE of 0.47°C (Figure 19c). RMSE of the TriSonica when mounted on the tower was 0.42°C, comparable to that of the flights. These errors are well within the anemometer's temperature accuracy of ±2°C.

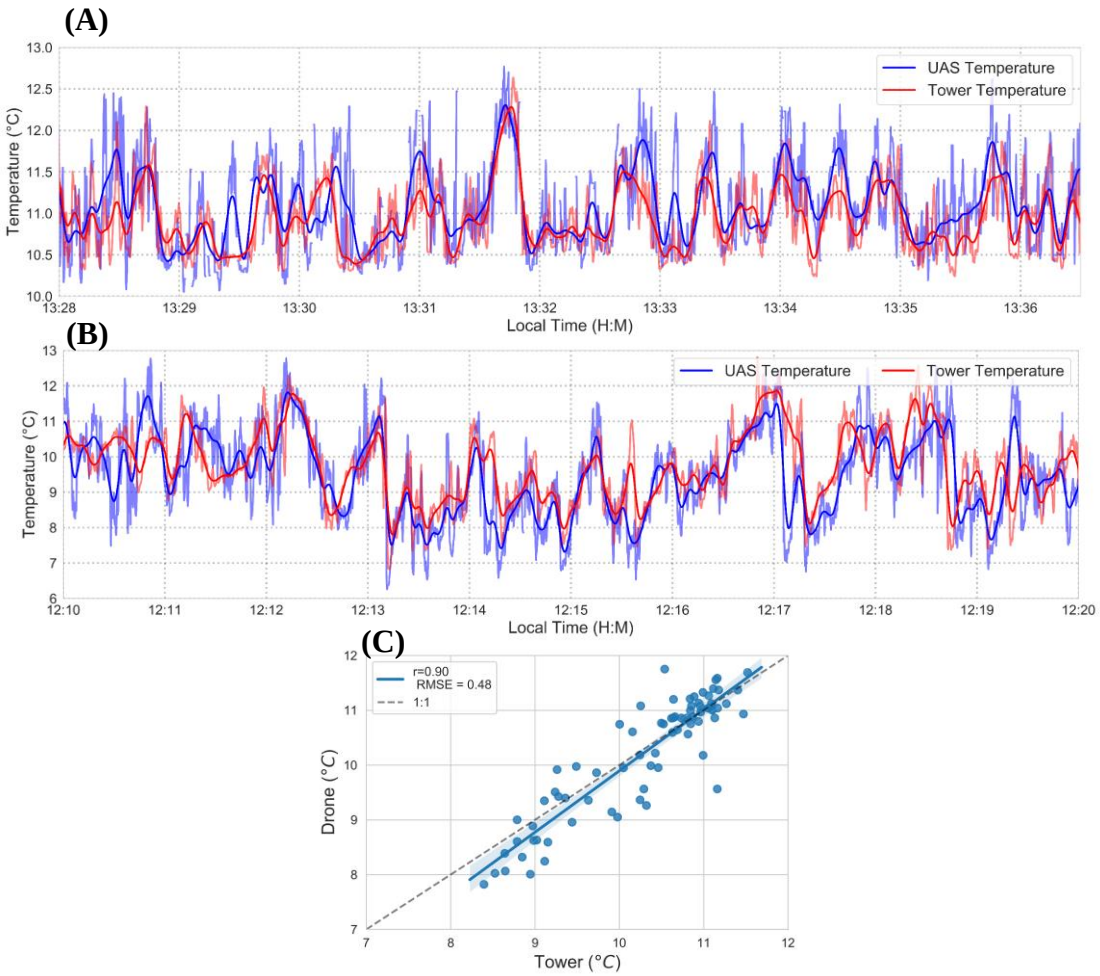

Figure 19. (A) Flight 1 time series of RMY and UAS sonic temperature in red and blue, respectively. Bold lines represent 15 second moving average with semi-transparent representing 1 second moving average. (B) Flight 2 time series of RMY and UAS sonic temperature in red and blue respectively with time averaging noted above. (C) Scatter plot of UAS sonic temperature versus RMY wind speeds for both flights in blue dots. Linear regression and 95% confidence interval in blue line and shading.

Section 5: Discussion

The use of UAS at wildland fires could be an improvement to the instrumentation currently available for monitoring the fire environment. UAS regulations are constantly changing, therefore the UAS operations at wildland fires will need to be consistently evaluated in order to keep up with these changes. However, UAS use at both wildland and prescribed fires will likely provide valuable information on local fire meteorology. These data can be used to calculate various fire-weather indices to provide fire behavior and smoke dispersion guidance. Our platform was able to perform high-resolution soundings, revealing small scale temperature and wind structures. Such observations may be missed or smoothed by radiosondes due to their faster ascent rate. Another reason UAS can be beneficial for observations in the fire environment is the ability to make multiple vertical profiles quickly reducing costs associated with balloons, sondes, and helium. UAS based sounding systems may prove to be more cost effective and user friendly than radiosonde systems for fire weather monitoring and observations. Another advantage of UAS, is that users have control over the entire sounding process, unlike radiosonde balloons, which drift freely potentially impacting aircraft-based suppression operations.

This platform can also be useful as a mobile temporary weather station. The system can be quickly assembled and launched to hover for 10-15 minutes at any height and location within the pilots' visual line of sight. The current setup of our platform can provide wind speed and temperature with accuracy of ±1 m s^{-1} and 0.5°C, in addition to RH and pressure observations which can provide a number of other calculated variables.

When data were averaged to that of a typical automatic weather station this platform excelled in low-wind environments, with errors of 0.02 m s^{-1}, while in moderate wind conditions the errors were ~ ±0.5 m s^{-1}.

While this platform is useful for atmospheric soundings and weather station-like observations, its limitations prevent it from being useful for directly quantifying fire-atmosphere interactions. With errors (of 1 m s^{-1} or more) being common with this platform, it may be difficult to determine if changes in the winds are caused by fire-induced circulations or are errors introduced by the prop wash, blockage, or movement of the platform.

This study provides groundwork for future UAS use for atmospheric monitoring in the fire environment, however, further research is needed to better understand UAS operations in the operational environment during active wildfire suppression activities. Additionally, more field testing is required to test other aspects of the platform, such as comparisons of the system's vertical profiles against other vertical profiling technologies such as tethersondes, radiosondes, or sodar and lidar. This could provide insight into any errors caused by sensor response times, mixing caused by the rotor wash, and any influence the platform body may have on blocking of winds. Additionally, more flights next to towers may provide better insight into optimal placement of sensors on the platform to limit sampling errors. Continued research will hopefully allow for UAS to be a feasible option for quantifying fire weather conditions during wildfire and prescribed fire events, in addition to being used for fire-atmosphere interactions research.

References

Abatzoglou, J. T., R. Barbero, and N. J. Nauslar, 2013: Diagnosing santa ana winds in Southern California with synoptic-scale analysis. *Weather Forecast.*, **28**, 704–710, https://doi.org/10.1175/WAF-D-13-00002.1.

Albini, F., 1978: Estimating Wildfire Behavior. *USDA For. Serv. Gen. Tech. Rep. INT-30*,.

Appenzeller, C., and H. C. Davies, 1992: Structure of stratospheric intrusions into the troposphere. *Nature*, **358**, 570–572, https://doi.org/10.1038/358570a0.

Barbieri, L., and Coauthors, 2019: Intercomparison of small unmanned aircraft system (sUAS) measurements for atmospheric science during the LAPSE-RATE campaign. *Sensors (Switzerland)*, **19**, https://doi.org/10.3390/s19092179.

Bowers, C. L., 2018: The Diablo Winds of Northern California. San Jose State University, .

Brinkman, W. A. R., 1971: What is a Foehn? *Weather*, 230–240, https://doi.org/10.1002/j.1477-8696.1971.tb04200.x.

Byram, G. M., 1954: Atmospheric Conditions Related to Blowup Fires. *U.S.Department Agric. - For. Fires*, 42.

Cao, Y., 2015: *The Santa Ana Winds of Southern California in the Context of Fire Weather*.

——, and R. G. Fovell, 2016: Downslope windstorms of San Diego County. Part I: A case study. *Mon. Weather Rev.*, **144**, 529–552, https://doi.org/10.1175/MWR-D-15-0147.1.

——, and ——, 2018: Downslope Windstorms of San Diego County. Part II: Physics Ensemble Analyses and Gust Forecasting. *Weather Forecast.*, **33**, 539–559, https://doi.org/10.1175/waf-d-17-0177.1.

Cheney, N. P., and J. S. Gould, 1995: Fire growth in grassland fuels. *Int. J. Wildl. Fire*, **5**, 237–247, https://doi.org/10.1071/WF9950237.

Chilson, P. B., and Coauthors, 2019: Moving towards a network of autonomous UAS atmospheric profiling stations for observations in the earth's lower atmosphere: The 3D mesonet concept. *Sensors (Switzerland)*, **19**, https://doi.org/10.3390/s19122720.

Clements, C. B., and A. J. Oliphant, 2014: The California State University Mobile

Atmospheric Profiling System. *Bull. Am. Meteorol. Soc.*, 1713–1724, https://doi.org/10.1175/BAMS-D-13-00179.1.

Clements, C. B., and Coauthors, 2007: Observing the Dynamics of Wildland Grass Fires fireflux1. *Bull. Am. Meteorol. Soc.*, https://doi.org/10.1175/BAMS-88-9-1369.

Clements, C. B., and Coauthors, 2016: Fire weather conditions and fire-atmosphere interactions observed during low-intensity prescribed fires - RxCADRE 2012. *Int. J. Wildl. Fire*, **25**, 90–101, https://doi.org/10.1071/WF14173.

——, and Coauthors, 2019: The FireFlux II experiment: A model-guided field experiment to improve understanding of fire-atmosphere interactions and fire spread. *Int. J. Wildl. Fire*, **28**, 308–326, https://doi.org/10.1071/WF18089.

Cohen, J. E., and J. D. Deeming, 1985: The National Fire-Danger Rating System: basic equations. *Gen. Tech. Rep.*, 16

Deeming, J. E., R. E. Burgan, and J. D. Cohen, 1978: *National Fire-Danger Rating System*. 60 pp.

Durran, D. R., 1990: Mountain Waves and Downslope Winds. *Atmospheric Processes over Complex Terrain*, W. Blumen, Ed., American Meteorological Society, 59–83.

——, 2003: Downslope Winds. *Encycl. Atmos. Sci.*, 644–650.

Edinger, J. G., R. A. Helvey, and D. Baumhefner, 1964: *Surface Wind Patterns in the Los Angeles Basin During "Santa Ana" Conditions*. 100 pp.

Elston, J., B. Argrow, M. Stachura, D. Weibel, D. Lawrence, and D. Pope, 2015: Overview of small fixed-wing unmanned aircraft for meteorological sampling. *J. Atmos. Ocean. Technol.*, **32**, 97–115, https://doi.org/10.1175/JTECH-D-13-00236.1.

Fosberg, M., 1978: Weather in Wildland Fire Management: The Fire Weather Index. *Conference on Sierra Nevada Meteorology*, Lake Tahoe, CA, 1–4.

Fovell, R., and A. Gallagher, 2018: Winds and Gusts during the Thomas Fire. *Fire*, **1**, 47, https://doi.org/10.3390/fire1030047.

Garcia Diez, E. L., L. Rivas Soriano, F. De Pablo Davila, and A. Garcia Diez, 1994: An objective forecasting model for the daily outbreak of forest fires based on meteorological considerations. *J. Appl. Meteorol.*, **33**, 519–526

Goodrick, S. L., 2002: Modification of the Fosberg fire weather index to include drought. *Int. J. Wildl. Fire*, **11**, 205–211, https://doi.org/10.1071/wf02005.

Haines, D. A., 1988: A lower atmosphere severity index for wildlife fires. *Natl. Weather Dig.*, **13**, 23–27.

Houston, A. L., B. Argrow, J. Elston, J. Lahowetz, E. W. Frew, and P. C. Kennedy, 2012: The collaborative Colorado-Nebraska unmanned aircraft system experiment. *Bull. Am. Meteorol. Soc.*, **93**, 39–54, https://doi.org/10.1175/2011BAMS3073.1.

Kiefer, C. M., C. B. Clements, and B. E. Potter, 2012: Application of a mini unmanned aircraft system for in situ monitoring of fire plume thermodynamic properties. *J. Atmos. Ocean. Technol.*, **29**, 309–315, https://doi.org/10.1175/JTECH-D-11-00112.1.

Klemp, J. B., and D. K. Lilly, 1974: The Dynamics of Wave-Induced Downslope Winds. *J. Atmos. Sci.*, **32**, 320–339.

Kobziar, L. N., M. R. A. Pingree, A. C. Watts, K. N. Nelson, T. J. Dreaden, and M. Ridout, 2019: Accessing the Life in Smoke: A New Application of Unmanned Aircraft Systems (UAS) to Sample Wildland Fire Bioaerosol Emissions and Their Environment. *Fire*, **2**, 56, https://doi.org/10.3390/fire2040056.

Markowski, P. M., and Y. P. Richardson, 2010: Mountain Waves and Downslope Winds. *Mesoscale Meteorology in Midlatitudes*, John Wiley and Sons, 327–342.

Mcintyre, M., 1984: The ‘ suf zone ’ in the stratosphere. **9169**, https://doi.org/10.1016/0021-9169(84)90063-1.

Mcintyre, M. E., and T. N. Palmer, 1983: Breaking planetary waves in the stratosphere. **600**, 593–600.

Merino, L., F. Caballero, J. R. Martínez-De-Dios, I. Maza, and A. Ollero, 2012: An unmanned aircraft system for automatic forest fire monitoring and measurement. *J. Intell. Robot. Syst. Theory Appl.*, **65**, 533–548, https://doi.org/10.1007/s10846-011-9560-x.

Moran, C. J., C. A. Seielstad, M. R. Cunningham, V. Hoff, R. A. Parsons, Ll. Queen, K. Sauerbrey, and T. Wallace, 2019: Deriving Fire Behavior Metrics from UAS Imagery. *Fire*, **2**, 36, https://doi.org/10.3390/fire2020036.

Nelson, K., J. Boehmler, A. Khlystov, H. Moosmüller, V. Samburova, C. Bhattarai, E. Wilcox, and A. Watts, 2019: A Multipollutant Smoke Emissions Sensing and Sampling Instrument Package for Unmanned Aircraft Systems: Development and Testing. *Fire*, **2**, 32, https://doi.org/10.3390/fire2020032.

Palomaki, R. T., N. T. Rose, M. van den Bossche, T. J. Sherman, and S. F. J. De Wekker, 2017: Wind estimation in the lower atmosphere using multirotor aircraft. *J. Atmos. Ocean. Technol.*, **34**, 1183–1191, https://doi.org/10.1175/JTECH-D-16-0177.1.

Pleim, J. E., 2007: A combined local and nonlocal closure model for the atmospheric boundary layer. Part I: Model description and testing. *J. Appl. Meteorol. Climatol.*, **46**, 1383–1395, https://doi.org/10.1175/JAM2539.1.

Pleim, J. E., and Aijun Xiu, 1995: Development and testing of a surface flux and planetary boundary layer model for application in mesoscale models. *J. Appl. Meteorol.*, **34**, 16–32, https://doi.org/10.1175/1520-0450-34.1.16.

Potter, B. E., 1996: Atmospheric properties associated with large wildfires. *Int. J. Wildl. Fire*, **6**, 71–76, https://doi.org/10.1071/WF9960071.

Prichard, S., and Coauthors, 2019: The Fire and Smoke Model Evaluation Experiment-A plan for integrated, large fire-atmosphere field campaigns. *Atmosphere (Basel).*, **10**, https://doi.org/10.3390/atmos10020066.

Raphael, M. N., 2003: The Santa Ana Winds of California. *Earth Interact.*, **7**, 1–13,

Rolinski, T., S. B. Capps, and W. Zhuang, 2019: Santa Ana winds: A descriptive climatology. *Weather Forecast.*, **34**, 257–275, https://doi.org/10.1175/WAF-D-18-0160.1.

Samiappan, S., L. Hathcock, G. Turnage, C. McCraine, J. Pitchford, and R. Moorhead, 2019: Remote Sensing of Wildfire Using a Small Unmanned Aerial System: Post-Fire Mapping, Vegetation Recovery and Damage Analysis in Grand Bay, Mississippi/Alabama, USA. *Drones*, **3**, 43, https://doi.org/10.3390/drones3020043.

Shimura, T., M. Inoue, H. Tsujimoto, K. Sasaki, and M. Iguchi, 2018: Estimation of wind vector profile using a hexarotor unmanned aerial vehicle and its application to meteorological observation up to 1000 m above surface. *J. Atmos. Ocean. Technol.*, **35**, 1621–1631, https://doi.org/10.1175/JTECH-D-17-0186.1.

Skamarock, W. C., and Coauthors, 2008: A description of the Advanced Research WRF Version 3, NCAR Technical Note TN-475+STR. *Tech. Rep.*, 113, https://doi.org/10.5065/D68S4MVH.

Smith, C., B. Hatchett, and M. Kaplan, 2018: A Surface Observation Based Climatology of Diablo-LikeWinds in California's Wine Country and Western Sierra Nevada. *Fire*, **1**, 25, https://doi.org/10.3390/fire1020025.

Smith, R. B., 1985: On Severe Downslope Winds. *J. Atmos. Sci.*, **42**, 2597–2603.

Srock, A. F., J. J. Charney, B. E. Potter, and S. L. Goodrick, 2018: The Hot-Dry-Windy Index: A new fireweather index. *Atmosphere (Basel).*, **9**, 1–11, https://doi.org/10.3390/atmos9070279.

Werth, P. A., and Coauthors, 2011: Synthesis of knowledge of extreme fire behavior: Volume I for fire managers. *USDA For. Serv. - Gen. Tech. Rep. PNW-GTR*, **I**, 144, https://doi.org/10.2737/PNW-GTR-854.

Westerling, A. L., D. R. Cayan, T. J. Brown, B. L. Hall, and L. G. Riddle, 2004: Climate, Santa Ana Winds and Autumn Wildfires in Southern California. *EOS, Tansactions, Am. Geophys. Union*, **85**, 289–296.

Whiteman, C. D., 2000: *Mountain Meteorology : Fundamentals and Applications*. Oxford University Press,.

Zachariassen, J., K. Zeller, N. Nikolov, and T. McClelland, 2003: A review of the forest service Remote Automated Weather Station (RAWS) network. *USDA For. Serv. - Gen. Tech. Rep. RMRS-GTR*, 1–161, https://doi.org/10.2737/rmrs-gtr-119.